Increasing the quality factor of microcantilevers in a fluid environment

François Castonguay

Master of Science

Department of Physics

McGill University

Montreal,Quebec

2010-08-30

A thesis submitted to McGill University in partial fulfillment of the requirements of the degree of Master of Science

©François Castonguay, 2010

ACKNOWLEDGEMENTS

I would first like to take the time to thank my supervisor, Prof. Peter Grütter, for his ingenuity and guidance throughout this project. His flexibility and trust have left me with a positive perception of academia and the physics department at McGill. This project would not have been possible without the undivided attention of Dr.Yoichi Miyahara and the other post-doc and research associates from our group, namely Dr. Helene Bourque, Dr. Yoshihiko Nagai and Dr. Aswin Lal. I can not forget to mention our other group members who were all very receptive anytime I had a question, and obviously making sure not to omit our ”part-time” group member James Hedberg for our numerous discussions on my project.

I also would like to thank Prof. Srikar Vengallatore and his group members Sairam Prabhakar and Guru Sosale, for their help in the theoretical explanation and setting up the project.

I could not have done much in the clean room without the help Dr. Matthieu Nannini, now fab manager, and dedicated technician Don Berry at the McGill Microfabrication facility.

Finally I would like to thank my parents for having been so supportive all these years. The beginning was rough, but I am eternally grateful for the end result!

ABSTRACT

The need to improve the quality factor of Atomic Force Microscopy cantilevers immersed in fluid has been demonstrated in great length, especially in the cases where samples need to be in their natural liquid environment. For that reason a series of low pressure chemical vapor deposited silicon nitride cantilevers were created based on a series of defined parameters. Each cantilever had a fixed surface area of $5600\mu m^2$, comparable with the rectangular cantilever of dimension of $140\mu m$ by $40\mu m$ used as a reference. A procedure to fabricate these levers in a clean room environment, as well as issues that came up during the fabrication, is explained in detail. Each measurement was done on our in-house setup. The main components of this apparatus are a focussed laser, a sample holder and a split photodiode. The results obtained were not as impressive as we had hope although some cantilevers showed a significant decrease in the quality factor, helping us direct future work on the subject. One cantilever (#9) did however show equivalent performance with respect to the reference cantilever and even slightly increasing the quality factor ratio in the second mode.

ABRÉGÉ

Le besoin criant d'augmenter le facteur de qualité de micros-levier immergée dans un fluide utilisé en microscopie de force atomique a été démontré a mainte reprise, plus particulièrement dans le cas ou les échantillons devais être dans leur environnent liquide naturelle. C'est pour cette raison qu'une série de micro-levier ont été crée sur une basse de paramètre prédéfini et avec un dépôt de nitrure de silicium chimique en phase vapeur sous pression réduite. Chaque micros-leviers a une aire de surface de $5600\mu m^2$, pouvant ainsi être comparé avec le micro-levier de référence ayant pour dimension $140\mu m$ par $40\mu m$. Une procédure pour fabriquer c'est micros-leviers dans un environment de salle blanche, ainsi que les méthodes utiliser pour contrevenir aux problèmes encourus durant la fabrication, sont expliqués en détail. Chaque prise de mesure a été effectué sur notre appareil fait maison ayant comment composante principale un laser focalisé, un porte échantillon et une photodiode diviseé. Les résultats obtenu n'ont pas été a la hauteur de nos attentes, néanmoins certain micros-leviers ont démontrés une réduction significative de leur facteur de qualité, nous aidant donc à diriger le travail futur sur le sujet. Un micro-levier (#9), a par contre démontré une performance équivalente par rapport au micro-levier de référence augmentant même le ratio de facteur de qualité pour le 2e mode d'opération.

TABLE OF CONTENTS

ACKNOWLEDGEMENTS ii

ABSTRACT iii

ABRÉGÉ iv

LIST OF TABLES vii

LIST OF FIGURES viii

1 Introduction 1

1.1 Principles of Atomic Force Microscopy 2
1.2 Motivation behind Non-Contact AFM in liquids 4
1.3 Thermal Noise 5

2 Theory 7

2.1 Resonance Frequency 7
2.2 Quality Factor 8
2.3 Damping 11

3 Previous Work 15

4 An Introduction to Microfabrication Techniques 17

4.1 Mask Fabrication 17
4.2 Photolithography 22
4.3 Etching 23
4.3.1 Dry Etching 24
4.3.2 Wet Etching 26
4.4 Process Flow 27
4.4.1 Photoresist Exposure 27
4.4.2 Silicon Nitride Etching 29
4.4.3 Silicon Etching 29

5 Characterization of microfabricated cantilevers 32
5.1 Under and Over Etch Silicon 32
5.1.1 Localized Over Etch 32
5.1.2 Localized Under Etch 33
5.2 Cantilever Robustness in Water 34
5.3 Bubbles 36
5.4 SEM Imaging 36
6 Experimental Results 39
6.1 Experimental apparatus 39
6.2 Software 41
6.2.1 Anti-Aliasing 43
6.2.2 Laser Position 44
6.3 Results 46
6.3.1 Resonance Frequency and Quality Factor 47
6.3.2 Cantilever Contour 56
6.3.3 Cantilevers Interference 56
7 Conclusions and Outlook 59
Appendix A 62
Appendix B 63
References 66

LIST OF TABLES

Table page

2–1 Numerical approximation for the value $\beta_i l$ 8

4–1 Contour of each cantilever. These are the sum of all the edges that will be in direct contact with the fluid and that are a possible source of drag or dissipation. Since every cantilever has the same surface area this value is of great interest. 19

6–1 Values for the reference cantilever in air 47

6–2 Values for the reference cantilever in air with an assumed Young's modulus of 190 GPa. 48

6–3 Values for the reference cantilever in water 48

6–4 Values for the modified cantilevers in air 49

6–5 Values for the modified cantilevers in water 50

6–6 Difference between reference and modified cantilever. The two cantilevers have the same contour dimension. The reference one is a simple rectangular cantilever whereas the modified one has special features. A negative number signifies that the resonance frequency on the modified cantilever is smaller than the reference one. 55

6–7 Difference between top and bottom matching cantilevers. This difference is calculated to ensure there is no coupling within neighboring cantilevers. 57

LIST OF FIGURES

Figure | page

1–1 A sketch of the basic components of an AFM. Not to scale 3

2–1 Shapes of the first four modes of a *fixed-free* cantilever. The red arrows show the nodes of each mode. 8

2–2 Explanation of the Quality factor, where the bandwidth is determined at half the maximum energy. 9

2–3 Example of different Q-factors 10

2–4 Typical result of the ring down method. A is the amplitude of the resonance, t is time and τ is the time decay constant 11

4–1 (A) Example of a die used for this project. The black part represents the region covered by silicon nitride and the white part would be etched away. (B) Magnified view of a set of 3 cantilevers 18

4–2 Sketch of cantilevers 1 to 6. Every cantilever has a constant surface area (black region) of $5600 \mu m^2$. This is obtained by changing the contour lengths, see table 4–1. Not to scale. 20

4–3 Sketch of cantilevers 7 to 12. Every cantilever has a constant surface area (black region) of $5600 \mu m^2$. This is obtained by changing the contour lengths, see table 4–1. Not to scale. 21

4–4 Photoresist exposure process. Not to scale 24

4–5 Diagram of a common RIE setup 25

4–6 RIE process illustrated for a photoresist mask on silicon nitride 26

4–7 Representation of isotropic and anisotropic etching 27

4–8 Simplified steps for the fabrication of a cantilever 31

5–1 Visual explanation of over etching 33

5–2 Visual explanation of over etching 34

5–3 A photographic image of partly immersed cantilevers 35

5–4 SEM images of microfabricated silicon nitride cantilevers 37

5–5 SEM images of microfabricated silicon nitride cantilevers 38

6–1 Home made sample holder 40

6–2 Picture of the experimental setup 41

6–3 Effect of aliasing. X axis is Hz. Y axis is a normalized arbitrary unit of intensity. Blue and red were collected at 1MHz and the green at 10MHz 44

6–4 1st mode of a base cantilever($\approx 28kHz$).The 3 colors represent different locations of the laser beam on the lever. Inset is a representation of the laser position on a cantilever. 45

6–5 2nd mode of a base cantilever($\approx 177kHz$). Same as above except that the second mode of the red line disappeared. 46

6–6 1st mode Q-factor and ratio. Top line is the Q-factor in air. The bottom line is the Q-factor in water. The middle line that uses the right y-axis is the ratio of Q-water over Q-Air. The dotted line is the same ratio but for the reference cantilever, and the grey area is the error attached to that number. 51

6–7 2nd mode Q-factor and ratio. Top line is the Q-factor in air. The bottom line is the Q-factor in water. The middle line that uses the right y-axis is the ratio of Q-water over Q-Air. The dotted line is the same ratio but for the reference cantilever, and the grey area is the error attached to that number. 52

6–8 Comparison between resonance frequency behavior and quality factor in both air and water for both modes. 54

6–9 Comparison between quality factor and contour length in both air and water for the second mode. 57

CHAPTER 1
Introduction

Being able to understand the very small has been the quest of the scientist for many years. With the concept of understanding came the craving to be able to see the smallest features of our universe. From the early beginnings of the microscope, invented in 1590 by Middelburg, to the 2008 Large Hadron Collider in Europe, the desire to be able to understand the world that lies beyond our eyes has remained.

Having the knowledge to be capable of seeing something small is intrinsically important, but being able to see actual relevant properties is something else. What we mean by that is if you try to measure the mechanical properties of a neuron, for example, and deposit it on a glass slide, you will be able to measure the properties of this cell using many different technologies, but will it be useful information? A cell in air will most likely not behave the same way as a cell in liquid, hence the interest to work on a method that evaluates the properties of a sample in its original, native environment. For biological samples, this is most often in a liquid.

A common technology that aims to achieve such a goal is the atomic force microscope (see section 1.1), more specifically the one where the sample is immersed in a liquid. This is where this work starts its path. Throughout this thesis we will carry the reader along a scientific path that will show our efforts to improve a specific aspect of this methodology. To be more specific, we will use the scientific knowledge

gathered from many previous studies on fluid immersed atomic force microscopy and show our efforts to try to improve this technology in a dire need of a breakthrough.

We propose to modify the shape of the cantilevers used during an experiment to improve the quality factor, a parameter greatly reduced during an experiment due to liquid viscosity (see section 2.2). We were able to construct twelve different models of cantilevers, along with some reference ones, to try to tackle this problem. The method used to create these levers in a clean room as well as the scientific reasoning behind the construction of each cantilever is documented in the following sections of this thesis.

Although no significant improvement has been noticed for any of the proposed models, it does not necessarily mean that the concept is erroneous, but that more work should be performed to ensure the conclusions of this work.

1.1 Principles of Atomic Force Microscopy

Atomic force microscopy (AFM) was invented at Stanford University, by Gerd Binning and his colleague in 1986[1]. This revolutionary technology arose from the development of scanning tunnelling microscopy (STM), developed in Zurich in 1980 by the same Gerd Binning and Heinrich Rohrer[2]. The AFM is a clever instrument which has broken many boundaries in science, allowing a better understanding of the atomic world.

Although its scientific accomplishments are quite remarkable, the overall concept of this device is fairly simple. A sharp tip, attached to a micro cantilever, is brought in close proximity to a surface of interest. Forces acting on the tip lead to a change in the mechanical properties of the cantilever, such as deflection or resonant frequency.

The cantilever maps the surface forces, thus topography, by interacting with the substrate, much like running ones finger over a surface to sense its structure. Due to the sharpness of the tip and its atomic proximity to the surface, atomic scale images are created [3]. The deflection of the cantilever is measured using a focussed laser reflected off the cantilever and onto a split photo diode . The difference signal of the split photo diode is proportional to the cantilever deflection, with a sensitivity better than $1pm$. A graphical explanation of the setup is shown in figure (1–1).

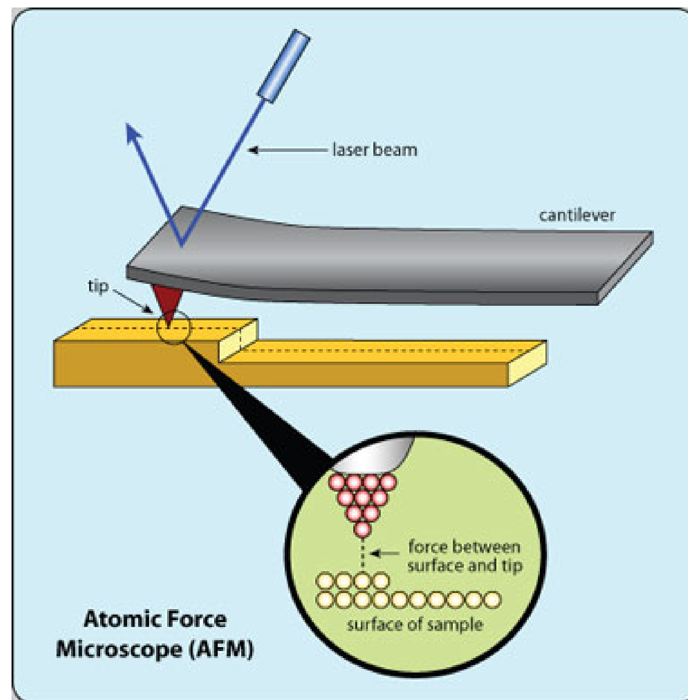

Figure 1–1: A sketch of the basic components of an AFM. Not to scale

There are two principle modes of operation in order to image a surface using an AFM; contact and non-contact mode[4]. In contact mode, also known as repulsive mode, a tip makes soft"physical contact" with the sample. The tip is attached to a

cantilever with a low spring constant. As the scanner gently sweeps the tip across the sample (or the sample under the tip), the contact force causes the cantilever to bend to accommodate changes in topography. Contact mode has the advantage of ease of use, simple electronics and high scanning speed on hard surfaces but can be destructive on softer ones.

1.2 Motivation behind Non-Contact AFM in liquids

In non-contact AFM (NC-AFM) the cantilever is vibrated and changes in either resonance frequency or vibration amplitude are electronically detected. The spacing between the tip and the sample for NC-AFM is on the order of one to hundreds of angstroms. NC-AFM allows the measurement of sample topography with little or no repulsive contact between the tip and the sample. Like contact AFM, non-contact AFM can be used to measure the topography of insulators and semiconductors as well as electrical conductors. The total force between the tip and the sample in the non-contact regime is very low, generally about 10^{-12}N. This small force is advantageous for studying soft or elastic samples. In the case of fluid measurements on soft samples the non contact mode most commonly used is the amplitude detection mode (known under the trade mark of Tapping Mode). More information about each mode and the AFM in general can be found in many books such as *Atomic Force Microscopy in Process Engineering* from Bowen et al.[2].

One field most particulary interested in this concept is the bio-physics world. Many papers have been published on the imaging of DNA, RNA or lipid bilayers and most of them comment that they would greatly benefit from a method to enhance the quality of their images (i.e. contrast and resolution, both related to the smallest

detectable interaction). We recommend having a look at Hansama et al.[5], that summarizes quite well the state of the technology in this field. The authors also point out the essential aspect of having an imaging tool in liquid. All this to say that the need to improve the imaging in solution is pressing and is looked at in many different research groups around the world.

1.3 Thermal Noise

In atomic force microscopy, the thermal vibrations of the cantilever is the limiting fundamental source of noise. The thermal noise of a lever can be calculated using the equipartition theorem [6]. The theorem states that if a system is in thermal equilibrium, the total energy E_{Total} of the independent quadratic term has a mean value equal to:

$$E_{Total} = \frac{1}{2} k_b T \tag{1.1}$$

where T is the temperature in kelvin and k_b is the Boltzmann constant. For small deflections z of the cantilever, its potential energy is $\frac{1}{2}Kz^2$, where K is the spring constant of the cantilever. Since we are working with a rectangular cantilever, here approximated as a spring, we use the following expression for the spring constant:

$$K = \frac{Ewh^3}{4L^3}, \tag{1.2}$$

where E is the elastic modulus (for Si_3N_4 a value of 290 GPa was used for this study), w the width, h the thickness of the cantilever and L the rectangular cross section. This equation was taken directly from Sader et al.[7], but is a commonly used equation for a rectangular beam. The equipartition theorem therefore becomes:

$$\frac{1}{2}k_bT = \frac{1}{2}\frac{Ewh^3}{4L^3}\widehat{z^2} = \frac{1}{2}K\widehat{z^2} \tag{1.3}$$

where the symbol $\widehat{z^2}$ represents the mean square deflection of the cantilever caused by thermal vibration. Knowing the type of cantilever we are dealing with, the equation can be rearranged in order to get an approximation for the amplitude of the thermal noise at room temperature:

$$\widehat{z^2} = \sqrt{\frac{k_bT}{K}} \approx \frac{0.64\mathring{A}}{\sqrt{K}}, \tag{1.4}$$

Since our spring constants are in the range of $0.1N/m$, we can calculate that the mean square deflection should be around $2\mathring{A}$, well within the range of our photo diode. Non-contact modes often favored in imaging soft samples (such as biological tissue) use an oscillating cantilever. The thermally limited minimal detectable frequency shift ($\frac{\delta f}{f}$), a direct measure of the tip-sample interaction, is inversely proportional to the square root of Q and given by

$$\frac{\delta f}{f} = \frac{\sqrt{2k_bTB}}{\sqrt{\pi^3kA^2fQ}}, \tag{1.5}$$

where T is the temperature, A the cross sectional area and B is the bandwidth. From this equation it is clear that a higher Q-factor will reduce the minimal detectable frequency shift, hence enhancing the quality of the results.

CHAPTER 2
Theory

In this chapter we will talk about some of the critical theoretical concepts involved in this project. This recapitulation of some basic and some not so basic theory aspects will help the reader to further extend his/her understanding.

2.1 Resonance Frequency

The resonance frequency of a cantilever can be easily approximated using differential mathematics and some basic boundary conditions. In this case we are mainly interested in the lateral vibration of the beam. The basic free equation is derived in a book from Singiresu S. Rao [8] and is shown in equation 2.1.

$$f_i = \frac{(\beta_i l)^2}{2\pi} \sqrt{\frac{EI}{\rho A l^4}} \tag{2.1}$$

In this equation f_i represents the ith resonance frequency, β depends on the boundary conditions (calculated numerical approximation and the value can be seen in table 2–1). E is the Young's modulus of the cantilever, I is the moment of inertia, ρ is the mass density of the cantilever, A is the cross-sectional area of the beam and l is the length of the lever.

The representation of these modes for a *fixed-free* cantilever can be seen in figure 2–1. The values calculated from equation 2.1 and table 2–1 give the resonance frequencies in a vacuum.

$\beta_i l$	Numerical approximation
$\beta_1 l$	1.875104
$\beta_2 l$	4.694091
$\beta_3 l$	7.854757
$\beta_4 l$	10.995541

Table 2–1: Numerical approximation for the value $\beta_i l$ for a cantilever with one fixed end and a free one[8].

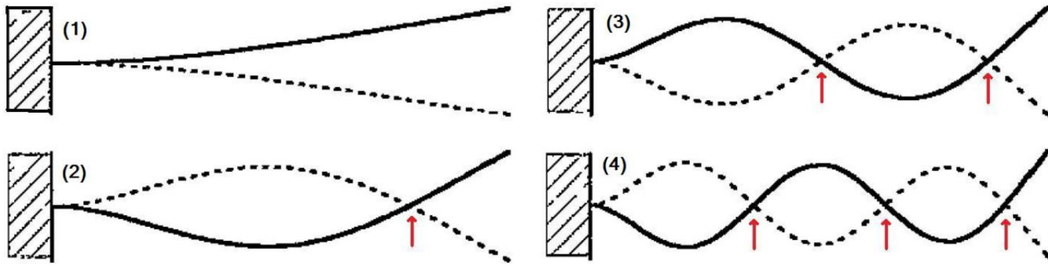

Figure 2–1: Shapes of the first four modes of a *fixed-free* cantilever. The red arrows show the nodes of each mode.

2.2 Quality Factor

The quality factor (Q-factor) is the value of the amplitude ratio at resonance of a system. It characterizes a resonator's bandwidth (Δf) relative to its resonance frequency, as shown in figure 2–2.

Generally the Q-factor is defined as the ratio of the energy stored to the energy lost per cycle, as shown in the equation below:

$$Q = \frac{\text{Energy Stored}}{\text{Energy dissipated per cycle}} \tag{2.2}$$

To put it in more mathematical terms, with the aid of figure 2–2, the following equation describes the quality factor:

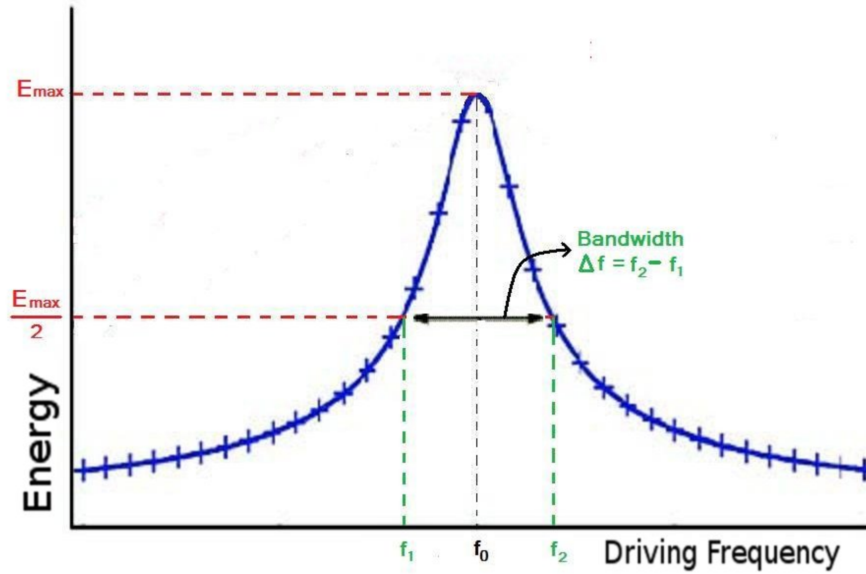

Figure 2–2: Explanation of the Quality factor, where the bandwidth is determined at half the maximum energy.

$$Q \approx \frac{f_0}{\Delta f} \tag{2.3}$$

A lower Q-factor indicates a higher rate of energy loss relative to the stored energy of the oscillator. In other words, the lower the quality factor, the quicker the oscillation amplitude will dampen out. A visual representation of this concept can be observed in figure 2–3.

Another common method of evaluating the quality factor experimentally involves exciting the cantilever at its resonance frequency and measuring the time it takes to decay to a certain level. The Q-factor can be calculated using the equation 2.4 where τ is the time decay constant and f the frequency of the sinusoidal driving

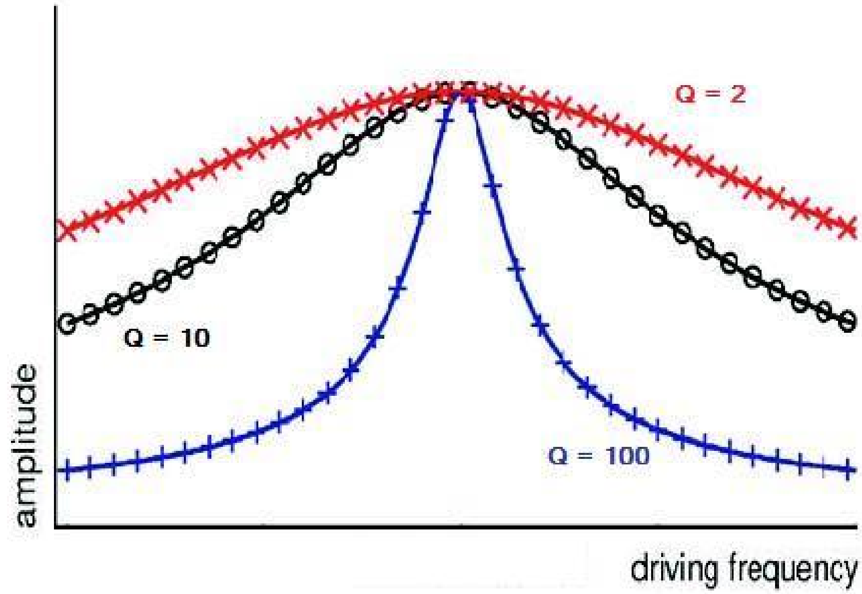

Figure 2–3: Example of different Q-factors

excitation, as shown in figure 2–4. The amplitude decays by $\frac{1}{e}$ ($\tilde{}\frac{1}{3}$) within a time of τ.

$$Q = \pi f \tau \tag{2.4}$$

So the idea is simply to increase the quality factor in order to decrease the energy loss of the cantilever, as shown in equation 2.5.

$$E_0(A) = \frac{\pi k A^2}{Q} \tag{2.5}$$

where E_0 is the intrinsic energy loss per oscillation cycle, A the oscillation amplitude and Q the quality factor [3]. From these key concepts it is clear that the medium in which the cantilever is immersed will greatly affect the value of the Q-factor of a

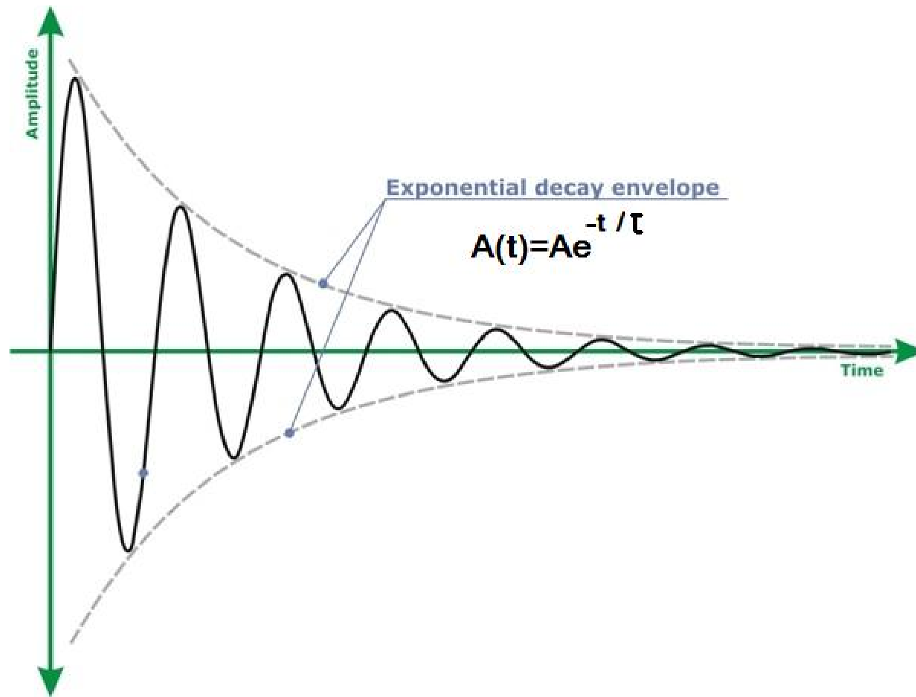

Figure 2–4: Typical result of the ring down method. A is the amplitude of the resonance, t is time and τ is the time decay constant

given lever [9]. This reduction in quality factor is a major problem for the resolution of the AFM as it creates a large decrease in force sensitivity of the apparatus. A low Q-factor will increase the minimum feature size that can be measured in modulated mode, hence counter balance the concept of measuring smaller features, as explained by equation 1.5.

2.3 Damping

Almost all physical systems, including cantilevers or other oscillating systems, are affected by friction or resistive forces. These forces tend to remove energy from a moving system and thereby slow it down or damp its motion. This universal fact is clearly very important for any physical system around us. For the pendulum to

maintain a given a amplitude, for example, energy must be supplied from, say, a wound spring or falling weights in order to maintain its complete amplitude.

What are the quantitative effects of these dissipative forces? We can answer this in the case of a drag force, $\vec{F}_d$, which is proportional to the velocity:

$$\vec{F}_d = b\frac{d\vec{x}}{dt} = -b\vec{v}, \tag{2.6}$$

where b is the damping coefficient. We can therefore, using the classical Hook's law, $F = -kx$, find the equation of motion for our damped cantilever, showed here in equation 2.7.

$$-kx - b\frac{dx}{dt} = m\frac{d^2x}{dt^2} \tag{2.7}$$

The solution to this equation is no longer simple harmonic motion and can be solved using simple differential equations. The standard result, solved with a Lorentzian, can be determined to be:

$$x(t) = Ae^{\frac{-bt}{2m}} sin(\omega_0 t), \tag{2.8}$$

where A is a constant defined by the function used, and ω_0 is the angular resonance frequency. It is important to notice here that the ratio $\frac{b}{m}$ is of great relevance and represents the inverse of the decay (τ) of the oscillation (explained in the next chapter), which is directly related to the quality factor introduced in section 2.2:

$$Q \equiv \omega\frac{m}{b} \equiv \omega_0\tau, \tag{2.9}$$

This brings to question why this damping or dissipation of energy occurs in the first place. We will present some of the aspects that are the cause of this shift in later sections. We do, however, want to point out that very little work has been done to improve the drastic drop in Q-factor in liquids, where many fields of study, such as mass sensing with cantilevers via resonance detection [10] or AFM imaging of biological systems in solution [11], for example, could benefit from any significant improvement.

For the interest of this work it is important to note that there is a great difference between frequency measurements conducted in a vacuum f_{vacuum} versus in a fluid environment f_{liquid}. It has been very well documented that the interaction of the cantilever with a medium greatly affects its resonance response [7,12-16].The most common equation used for a rectangular cantilever immersed in a fluid comes from Chu et al.[12] and is shown in equation 2.10:

$$f_{liquid} = f_{vacuum} \left(1 + \frac{\pi \rho_f w}{4 \rho_c t} \right)^{-\frac{1}{2}} \tag{2.10}$$

where ρ_f is the density of the fluid in which the lever is immersed (i.e zero for a vacuum), ρ_c is the density of the cantilever (i.e silicon nitride), w represents the width of the cantilever and t its thickness. In order for the equation to be valid the system must obey 5 basic rules: "1-The beam has a uniform cross section over its entire length; 2-The length L of the beam greatly exceeds its nominal width w; 3-The beam is an isotropic linearly elastic solid and internal frictional effects are negligible; 4-The amplitude of vibration is far smaller than any length scale of the beam; 5-The fluid is incompressible in nature" [12].

This equation is quite restrictive and does not take the length into consideration as it is theoretically valid for infinitely long cantilevers. Its validity beyond the first resonance mode is of no great accuracy. It is for that reason that other models have been proposed as a replacement or with corrective factors. The most famous one is from Sader et al.[7] and can be seen in the following equation:

$$f_{liquid,n} = f_{vacuum,n} \left(1 + \frac{\pi \rho_f w}{4 \rho_c t} \Gamma_r(\omega_n)\right)^{-\frac{1}{2}} \tag{2.11}$$

In this case the frequencies are now dependent on the mode, n, the function $\Gamma(\omega)$ is called the "hydrodynamic function" and is strongly dependant on the cross section of the beam and the Reynolds number, *Re.* An explicit analytical expression for $\Gamma(\omega)$ for a beam of similar appearance as our reference cantilever is given in a previous paper from Sader [13]. Since our levers of interest do not have a constant cross section and hence do not fulfill one of the 5 assumptions leading to Chu's equation mentioned above, the theoretical comparison of each of our levers will not be strictly possible using either formula.

A quick calculation, however, of the difference in frequencies will probably give a better perspective to the reader. For example, a cantilever immersed in pure water or isopropanol will have its resonant frequency reduced by 80% and 76%, respectively. This lowering is mainly caused by two major factors: mass loading and viscous drag, both crucially important in equation 2.11 as the drag component is incorporated in the hydrodynamic function.

CHAPTER 3
Previous Work

This project was instigated by Duan Xuefeng, a previous student in our group. His previous designs were based on lengthy fluid mechanics calculations and complicated CAD designs. The details of his work will not be covered here, but more information can be easily accessed via his former work [17]. We will however try to explain the basic concepts behind his design.

Most of his work was based on two papers, by Fukuma et al. in 2005 [18] and 2006 [19]. The authors talk about the fact that most high-resolution FM-AFM images were only previously obtained in ultrahigh vacuum (UHV) environments. Working in UHV restricts users from many practical applications such as measurements in fluid. In particular, imaging in liquid is crucial to survey biological samples such as DNA, proteins and living cells in an environment that resemble their natural habitat [18]. The authors also point out the key problem in imaging in fluid is a reduced quality factor. From this, they propose creating a low noise cantilever deflection sensor system that would work in multiple environments. One of their conclusions was that lowering the noise is a key aspect in being able to measure live samples in a fluid environment, but also note another way to increase the Q-factor could be to modify the shapes of the cantilevers themselves [18].

Now that the need for different cantilever design was exposed, many studies were used to developed these enhanced levers. The first point that had to be ensured was

that the cantilevers evaluated were of the appropriate spring constant, K, to measure biological samples. For that purpose, the paper from Walters et al.[20] provides a suitable guideline. It emphasized the importance of different key aspects to optimize a cantilever used in force modulated mode.

Another aspect covered in the creation of the original cantilevers is the evaluation of the spring constant of each cantilever. In order to be able to evaluate each modified cantilever in a way that would ensure meaningful results, one has to create levers with spring constants as similar as possible to each other, and for that purpose another paper from Sader et al. was used [21]. Many other papers by Sader dealing with various shapes of cantilevers in fluids were also used during this project [7,9,13], in helping the authors of this work understand the intrinsic behavior of immersed cantilevers.

The last issue considered was enhancing the quality factor of the modified cantilever despite the increased viscosity. Since the lever would be in direct contact with some fluid, it was crucial that we understand the physics behind this interaction. For this purpose, the work of Oden et al. is illuminating [22]. They showed experimental results of commercially available cantilevers affected by different fluids and presented reasonable quantitative agreement between experiments and models based on fluid dynamics. We therefore applied these models to create the cantilevers described in section 4.1.

CHAPTER 4
An Introduction to Microfabrication Techniques

In this chapter we will cover the basic concepts used to fabricate the micro-cantilevers. The entire process was done in a cleanroom at the *McGill Nanotools Microfab*. Twenty five 6 inch, prime <100>silicon wafers, polished on both sides, were purchased from *Montco Silicon Technologies Inc.*. Each wafer had a thickness between 600 and 700μm and an added layer of 5000$\AA \pm 5\%$ of a low pressure chemical vapor deposition (LPCVD) silicon nitride (Si_3N_4).

4.1 Mask Fabrication

A series of different cantilevers were created using a CAD-like software[1] especially designed for microfabrication mask fabrication. Each six inch wafer has 37 dies, shown in figure4–1(A) and each die would have 12 chips. To ensure a certain cantilever stability, eight holders were placed in strategic locations to ensure the maximum strength of each individual chip.

On each of these chips, six cantilevers have been placed in two sets of three, one of which is shown in figure 4–1(B), for a total of 2664 cantilevers per wafer. The top and bottom cantilevers are mirror images of each other with the only difference being the spacing between each of them. For the top set of cantilevers a separation distance

[1] CleWin is a layout editor designed in cooperation with the MESA+ Research Institute at the University of Twente and Deltamask, a mask making company.

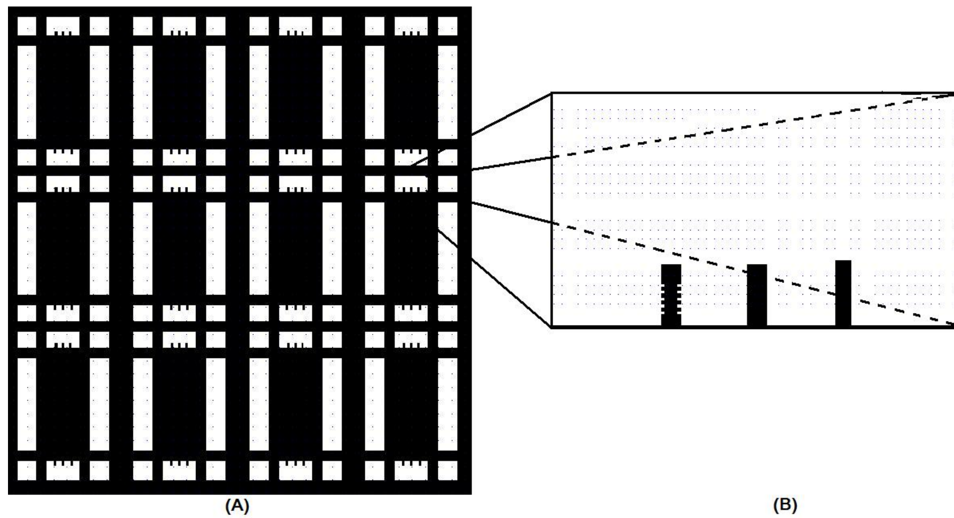

Figure 4–1: (A) Example of a die used for this project. The black part represents the region covered by silicon nitride and the white part would be etched away. (B) Magnified view of a set of 3 cantilevers

of $170\mu m$ was selected to ensure an equal distance between the wall of the die and each cantilevers. The bottom ones are separated by $205\mu m$, a distance selected to maximize the space of the die without being too close to the sides hence avoiding interaction with the borders. This was implemented to ensure and test that there was no coupling between the cantilevers when measurements were taken on individual levers.

As for the sets of 3 cantilevers, the patterns throughout the mask follow a consistent sequence. The cantilever positioned on the far right is called the *reference* cantilever and will have the same dimensions for each chip. This enables its use as a reference measurement for each individual die and chip to compensate for various inhomogeneities such as thickness or density that could, for example, occur on such a large surface or with different wafers. The width was set to $40\mu m$ and the length

to $140\mu m$, giving a target resonant frequency in vacuum of $38.1kHz$, thereby making a simple rectangular cantilever which allows for comparison with previous studies.

The left cantilever is called the cantilever of *interest*. This cantilever will be modified and is where most of the attention of this thesis will be focused on. A table of the different contour lengths is shown in table 4–1 and a sketch of these same twelve cantilevers of interest is shown in figures 4–2 & 4–3.

Contour of each cantilever	
Cantilever	Contour(μm)
1	500
2	870
3	994
4	482
5	522
6	660
7	430
8	510
9	416
10	480
11	642
12	962

Table 4–1: Contour of each cantilever. These are the sum of all the edges that will be in direct contact with the fluid and that are a possible source of drag or dissipation. Since every cantilever has the same surface area this value is of great interest.

As mentioned above, this project was instigated by Duan Xuefeng and the design of our cantilevers was based on his work. We did, however, work on one different aspect during this project and this aspect is symmetry. After spending some time on the previous work, we realized that the former designs were lacking symmetry

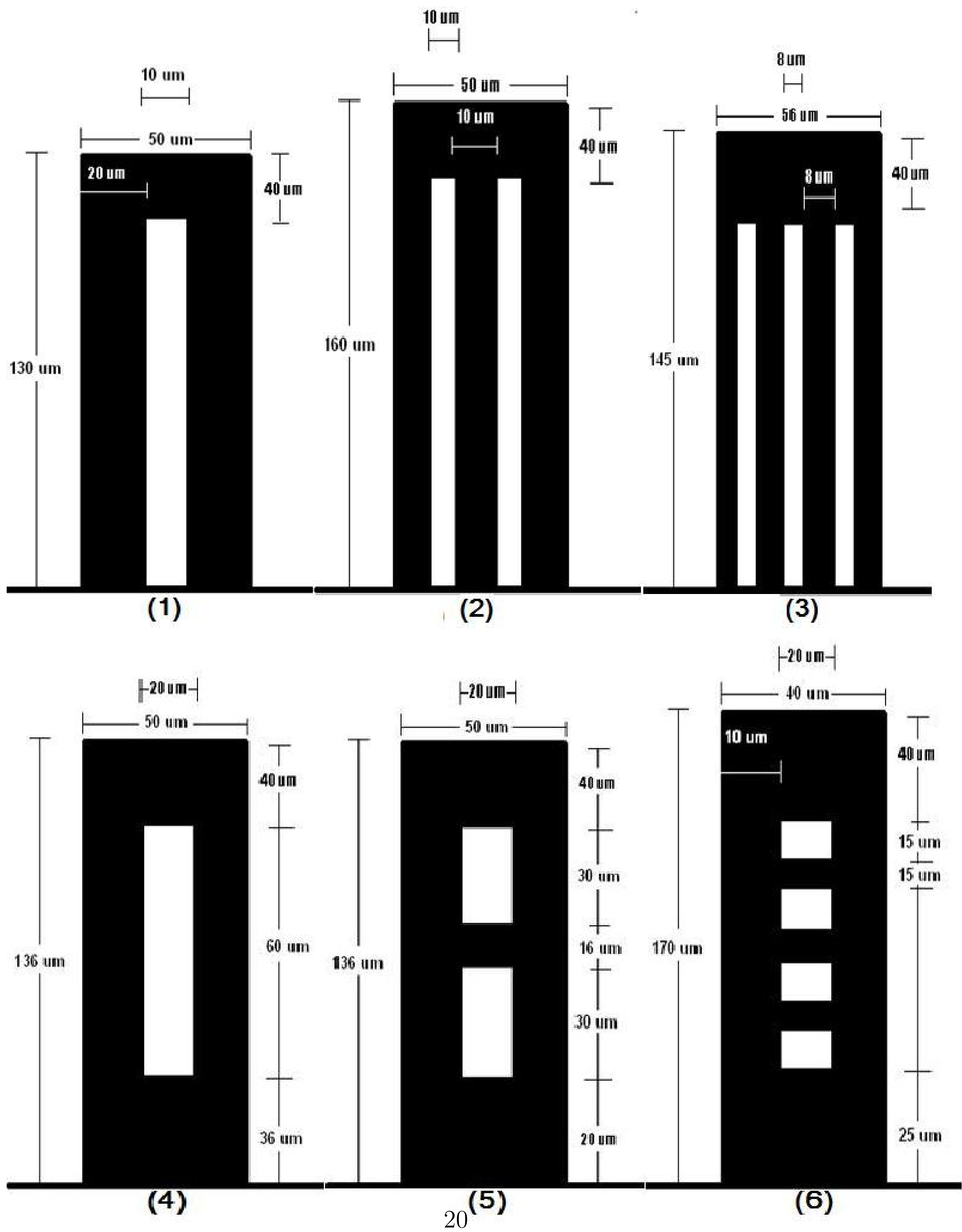

Figure 4–2: Sketch of cantilevers 1 to 6. Every cantilever has a constant surface area (black region) of $5600\mu m^2$. This is obtained by changing the contour lengths, see table 4–1. Not to scale.

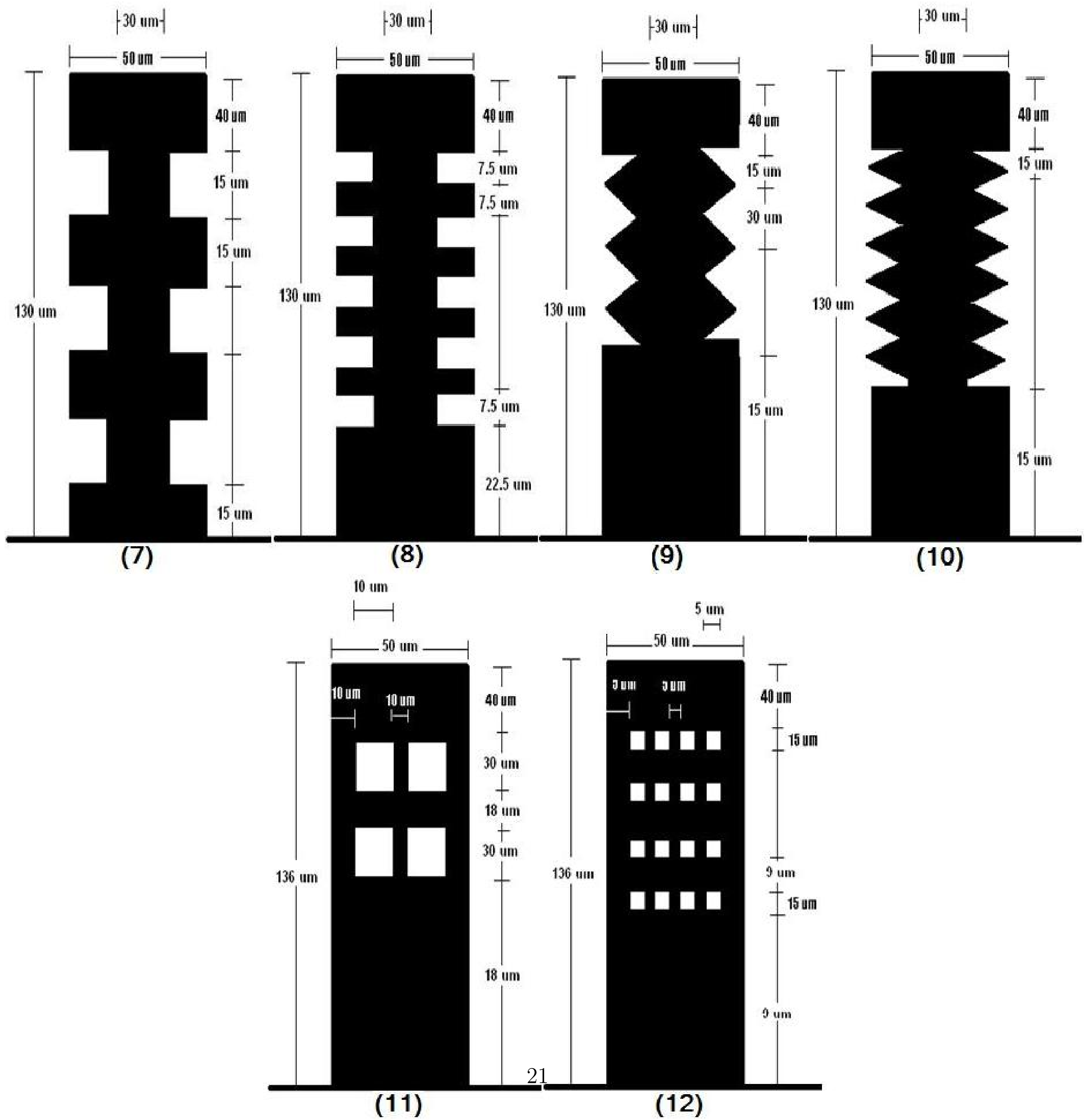

Figure 4–3: Sketch of cantilevers 7 to 12. Every cantilever has a constant surface area (black region) of $5600\mu m^2$. This is obtained by changing the contour lengths, see table 4–1. Not to scale.

and therefore addressing and convoluting too many aspects at the same time. Furthermore, the absence of a reference cantilever and potentially a lack of homogeneity across a wafer could have been the reason why the previous work was inconclusive. We therefore decided to reduce the complexity by including more symmetry in the designs of each type of cantilever, which also meant to eliminate some of the less important features in addition to adding a reference cantilever to each island.

Finally, by having different dimensions as compared to the reference cantilever, the lever of interest will obviously exhibit different behavior that may not be in relation to the features on the cantilevers, but simply due to its contour length. The middle cantilever was therefore introduced to verify this concept by having the same contour dimensions as the cantilever of interest. The middle cantilever will be a reference once again, but this time will be used to make sure the features on the cantilever of interest are making a difference. It can subsequently be compared to the cantilever of interest to see whether some features are more interesting than others. Some examples of CAD files can be found in Appendix A.

4.2 Photolithography

Once the CAD file was complete, it was sent to *HTA Photomask* to transfer the pattern from the file to a 7 inch chrome coated glass mask. This photolithography mask will be used to transfer the pattern onto the silicon nitride membrane. In order to achieve this task, a layer of photosensitive polymer, or photoresist (PR), was applied uniformly on the entire wafer using the *Spinball site coater* and a *Shipley 1813* positive photoresist. A recipe has been created to ensure the most uniform thickness with this type of PR. The wafer is held by the vacuum chuck of the *Spinball* and PR

was dispensed and spun at 3950 rotations per minute for 30s. Following this, the wafer is baked at 115°C for 1 minute to harden the PR. The approximate thickness of the deposited photoresist should be 1.4 μm thick after this last step[4]. It is important to note that the precise thickness is not crucial as the resist is only there to protect features in later steps, however non-uniformity will make it more difficult for a proper exposure as we are working very close to the mask during to the alignment.

The coated wafer was then put under *close proximity*, also called hard contact, to avoid diffraction effects from the light source. The mask was then exposed to an ultraviolet (UV) light source, hence attacking all the unprotected photoresist using the *EVG 620*, a dual-use tool designed for optical double-side lithography and precision alignment up to 6 inch wafer sizes. The photoresist was then exposed to enough energy, determined from calculations involving the type of PR, the wavelength of the light source and the intensity of the bulb. Once the exposure was complete,the wafer was developed using a chemical solution that removed photoresist that has been exposed to light[4]. A developer suitable for use with positive photoresist is based on a buffered aqueous-alkaline solution containing non-ionic surfactants and contains in the solution 1-100 part per million (ppm) of the surfactants, preferably of the ethoxylated-alkylphenol type[23].This entire process can be better understood using the visual aid of figure 4–4.

4.3 Etching

In this section we will be talking about the main etching methods used in the Microfab here at McGill. Dry etching 4.3.1 is the other main etching technique where the material is sputtered or dissolved using reactive ions or a vapor phase etchant.

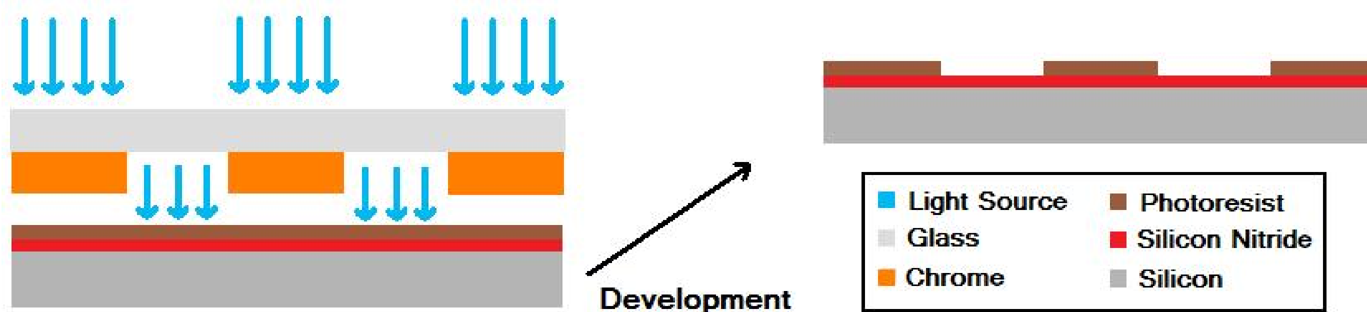

Figure 4–4: Photoresist exposure process. Not to scale

Wet etching 4.3.2 is a technique where the material is dissolved when immersed in a chemical solution.

4.3.1 Dry Etching

Once the exposed resist has been removed and the silicon nitride exposed, we used a reactive ion etcher (RIE) to etch away Si_3N_4. The RIE offers the possibility to set up anisotropic etching recipes using the common tool 5K. The selectivity of the etching will be greatly dependent on the material to be etched. Contamination is always an issue and is the reason why there are four different chambers in the RIE used in the Microfab, each with different etching purposes. Materials that are characterized by a high capacity to adsorb electrons are ideal candidates for highly anisotropic recipes, an example of which are semiconductors. In fact, anisotropic etching recipes concern mainly silicon, polysilicon and silicon nitride. This means that it will bombard the exposed Si_3N_4 but will be blocked by the photoresist, an organic material, hence leaving the features underneath intact[24].

Figure 4–5 shows a diagram of a common RIE setup. A reactive ion etcher consists of two electrodes (1 and 4) that create an electric field (3) with the purpose of accelerating ions (2) toward the first few layers of the sample (5).

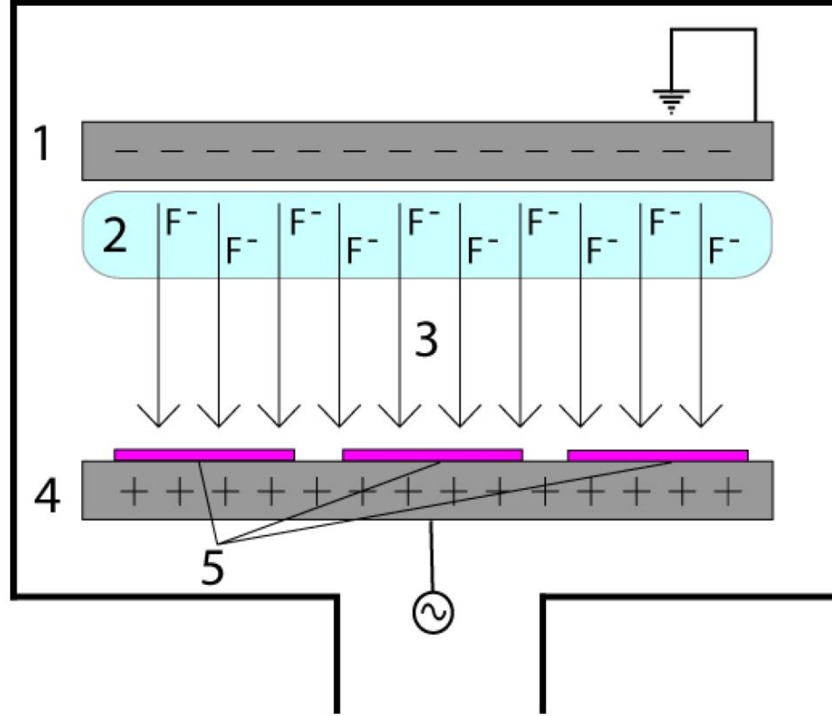

Figure 4–5: Diagram of a common RIE setup[25]

The area labelled (2) represents plasma that contains both negatively and positively charged ions in equal proportion. These ions are generated from the gases that are injected into the chamber. For the purpose of this experiment, we used chamber A, a chamber especially made for nitride etching that uses O_2 and CF_4 gasses for bombarding. In the diagram CF_4 has been pumped into the chamber, making a plasma with many fluorine ions (F^-). The fluorine ions are accelerated in the electric field, which causes them to collide into the surface of the sample.

Figure 4–6 shows a photoresist mask on silicon nitride. The etching ions are accelerated into the etching region, where they combine with silicon nitride and then are dispersed. Since the electric field accelerates ions toward the surface, the etching caused by these ions is much more dominant than the etching of radicals - ions travelling in varied directions, and therefore the etching is anisotropic [25].

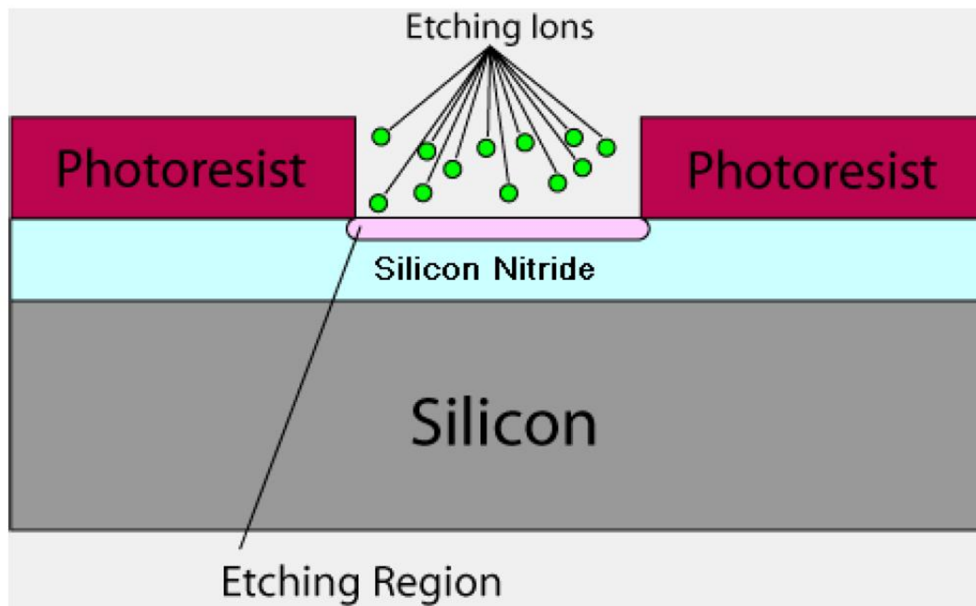

Figure 4–6: RIE process illustrated for a photoresist mask on silicon nitride[25]

4.3.2 Wet Etching

Wet etching is probably the simplest etching technology. It theoretically only requires a container and a chemical solution that will dissolve the material. Unfortunately, complications usually arise from the protective layer used to selectively etch the material. One must find a mask that will not dissolve or at least have a much slower etch rate than the material to be patterned. Secondly, some single crystal materials, such as silicon, exhibit anisotropic etching in certain chemicals.

Anisotropic etching in contrast to isotropic etching means different etch rates in different directions in the material. The classic example of this is the <111>crystal plane sidewalls that appear when etching a hole in a <100>silicon wafer in a chemical such as Tetramethylammonium hydroxide (TMAH), used for this process. The result is a pyramid shaped hole, with known angles, instead of a hole with rounded sidewalls when using an isotropic etchant. The principle of anisotropic and isotropic wet etching is illustrated in figure 4–7[26].

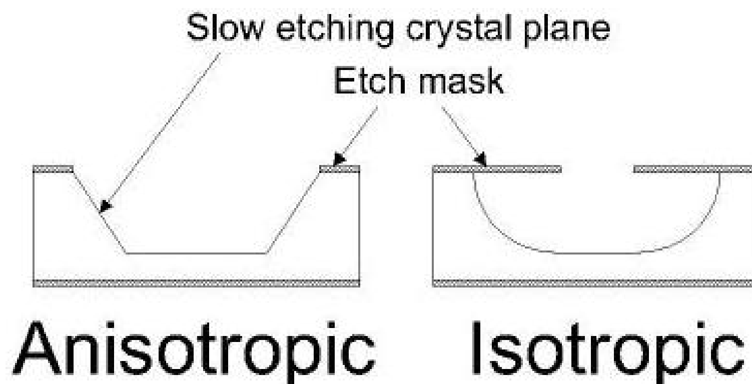

Figure 4–7: Representation of isotropic and anisotropic etching[26]

4.4 Process Flow

The process flow is the core of microfabrication work. Each batch of cantilevers produced has to go through a very specific order of events to assure quality and consistency. In this section we will go through the specifics of each step involved in the creation of levers.

4.4.1 Photoresist Exposure

In order to assure the most uniform layer of PR on the wafer, each wafer has to be cleaned and its thickness measured before any further steps are taken. The

cleaning process is a standard method at the Microfab and involves soaking a wafer in a beaker of acetone. This beaker is then put in an ionic bath at $80°C$ for 10 minutes. The process is then repeated replacing the acetone with isopropanol and finally water. The *Verteq rinser/dryer* was used to uniformly dry every 6 inch wafer.

As mention in section 4.2, the Spinball site coater was used to deposit the photoresist on the silicon nitride layer. We, however, realized after many trials that the addition of an adhesion layer between the PR and the wafer gave better results along the way. We therefore used a small layer of Hexamethyldisiloxane (HMDS) prior to coating the wafer with PR. It is important to realize that the coater used is not perfect and that every visibly non-uniform layer of photoresist had to be removed and the cleaning process had to be started all over again. Any defect in the PR deposition will directly affect the yield ratio of the cantilevers.

The first layer or the top mask is a relatively easy task using the *EVG 620*. Parameters have to be set depending on the type of PR, the thickness and the type of mask. In our case we calculated that $60mj/cm^2$ was the ideal intensity to optimize the exposure. The major issue arises from subsequent layers. As can be seen in the process flow, more than one mask is used to produce the cantilevers. Both the top and the bottom can not be etched at the same time and they also have different features. This means that an alignment between the front and the back side has to be done in order for the features from the front and from the back to coincide with each other. Although the *EVG 620* has the ability to achieve such a task, this is by far the most complicated part of the process flow.

4.4.2 Silicon Nitride Etching

As mentioned is section 4.3.1, the etching of the silicon nitride is done using the 5K, a reactive ion etcher. A recipe was developed to optimize the etching of the silicon nitride using multiple parameters, such as type of gas (CF_4,CHF_3) , pressure, time and magnetic field strength. As the chamber gets contaminated after every use and since this is a multi-user facility, new parameters had to be set for every use to stabilize the process. This means that before any etching of the actual sample, a clean wafer had to be put in and tested in order to find the current state on the machine and hence the parameters to be used. As you will see in the process flow, only the time was changed on every run in order to keep a certain aspect constant, such as the gas ratio. After each etching procedure, a measurement of the remaining layer was done on the sample to assure the complete removal of the layer on top of the silicon. After over 400 samples we can say with confidence that the etching uniformity of the 5K using our recipe is more than 97%.

4.4.3 Silicon Etching

The etching of the silicon is done in a bath especially made for this function. The solution consists of TMAH at 25% per volume heated to 85°C. Once again, the etch rate of the bath varies depending on how many etches have been done in the solution. For this reason, prior to every complete etch (i.e. etching of the entire silicon layer), a new bath was requested and a fresh TMAH solution was poured into the bath. Since most complete etches take more than 24 hours, it is easy to understand that the etching power of the solution decreases with time, hence creating potential issues (see section 5.1).

One last point to worry about when using the TMAH bath is the layer of native oxide that accumulates in between steps. Since this entire process is not all done under vacuum, particles of oxide adhere to the wafer and change the chemical composition of the first few layers. The TMAH will eventually break this weak bond and move on to the etching of the silicon. Due to this effect, however, the etch rate test should be done in the following manner. The wafer should be placed in the solution at the proper temperature then taken out after an hour and rinsed. Subsequently, the profilometer should be used to evaluate the height between the top of the nitride layer and the bottom of the etched silicon. Simply repeat the process once or twice to get an accurate measure of the silicon etching rate, usually ranging between 20 and $30 \mu m/hour$. A quick hydrofluoric acid (HF) dip is highly recommended before any TMAH etching. This entire etching process can be visualized in figure 4–8.
An example of a detailed process flow can be find in Appendix B.

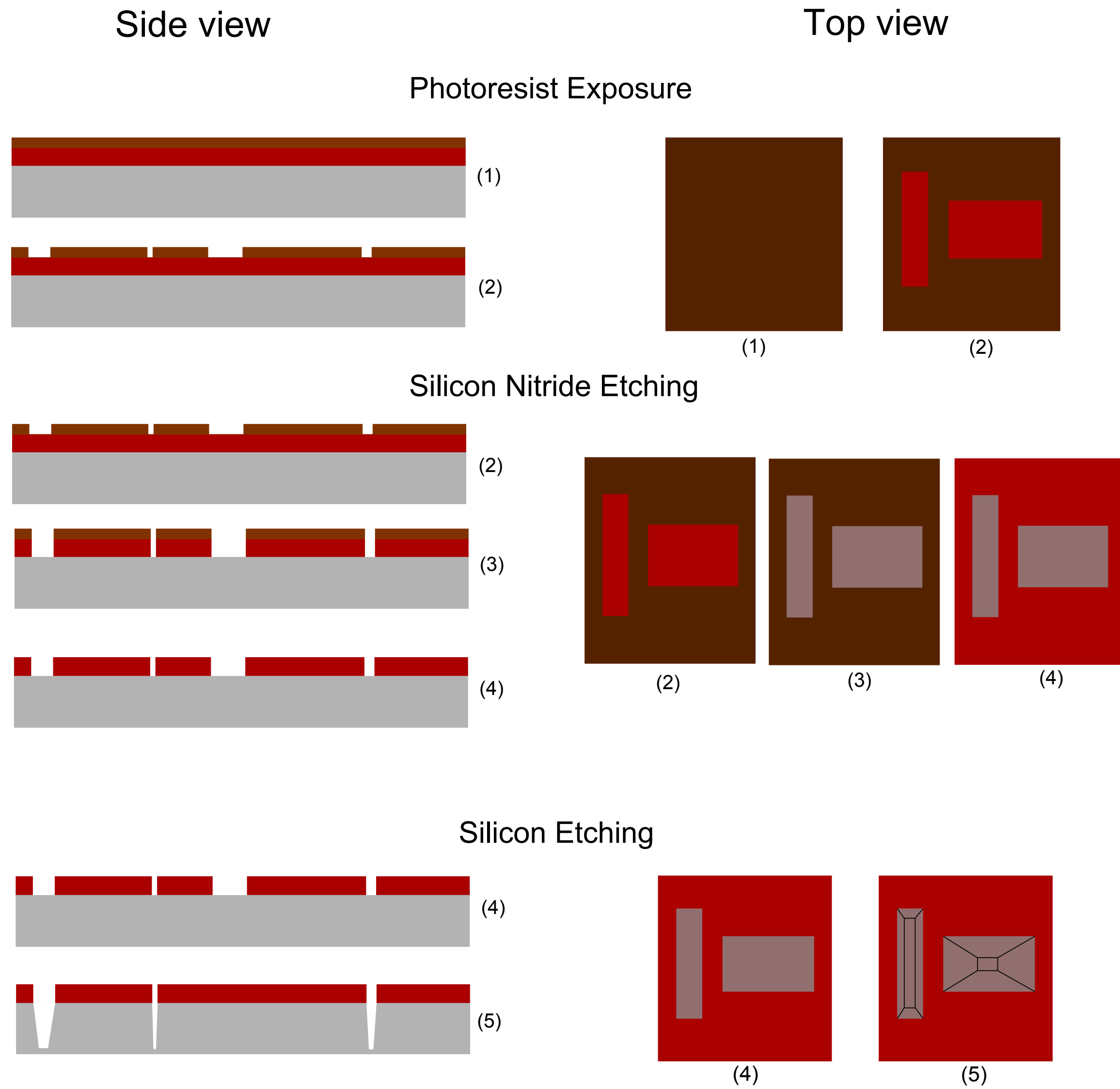

Figure 4–8: Simplified steps for the fabrication of a cantilever

CHAPTER 5
Characterization of microfabricated cantilevers

In this chapter we will talk about some issues that arose during the fabrication and the measurement of the cantilevers and the techniques we used to solve or improve some of these problems.

5.1 Under and Over Etch Silicon

The greatest problem that we faced in making the cantilevers came from the TMAH bath. The issue with this wet chemical etchant came from the flow of the fluid. Once immersed in the fluid, the six inch wafer was subject to the random flow of the bath and although the wafer was turned every two hours during the 24 hour etching period, it is clear that not all regions were etched evenly. This causes two main consequences, one being a localized over-etch the second one an under-etch.

5.1.1 Localized Over Etch

Over etching occurs when a specific location of the wafer is left too long in the TMAH and the normally very selective etchant starts etching other planes of the crystal. Figure 5–1 was added with the intention to help illustrate this concept to the reader.

This effect can be easily avoided by simply removing the wafers from the solution at an earlier time, but this could not be performed because of the too frequent occurrence of under etching.

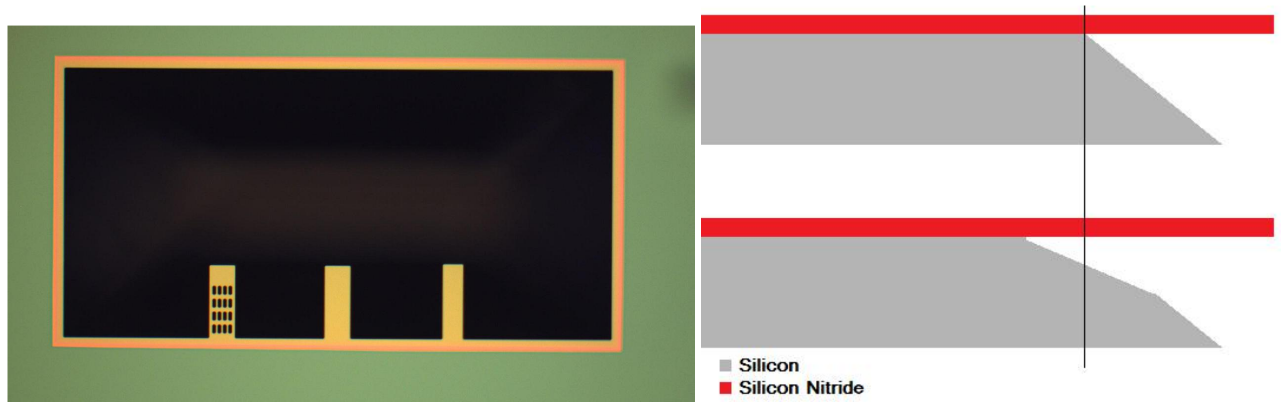

(a) Picture of an over etched set of cantilevers. The orange region is overhanging Si_3N_4

(b) Sketch of a side view of an over etched process. The black line represents the expected location of the silicon that coincides with the location of the etch nitride.

Figure 5–1: Visual explanation of over etching

5.1.2 Localized Under Etch

Under etch occurs in locations with less flow (i.e. in the deepest etching region), where it is hard for the fresh chemical to replace the old, less effective, etchant (see figure 5–2).

A new device was also added to improve the flow of chemical in the bath but did not show any significant improvement. This simple device stirred the water hoping to improve the overall flow over the surface of the wafer. The problem was that the stirrer could not be too strong as it would otherwise break the fragile cantilevers. The key is therefore to evaluate when to remove the wafers as a function of under etch versus over etch. Hence, we had to often remove and rinse the wafer near the end of the expected etching time in order to evaluate all locations and decide when to terminate the chemical etching, at the point where both reaction are minimized. A concept easier said than done!

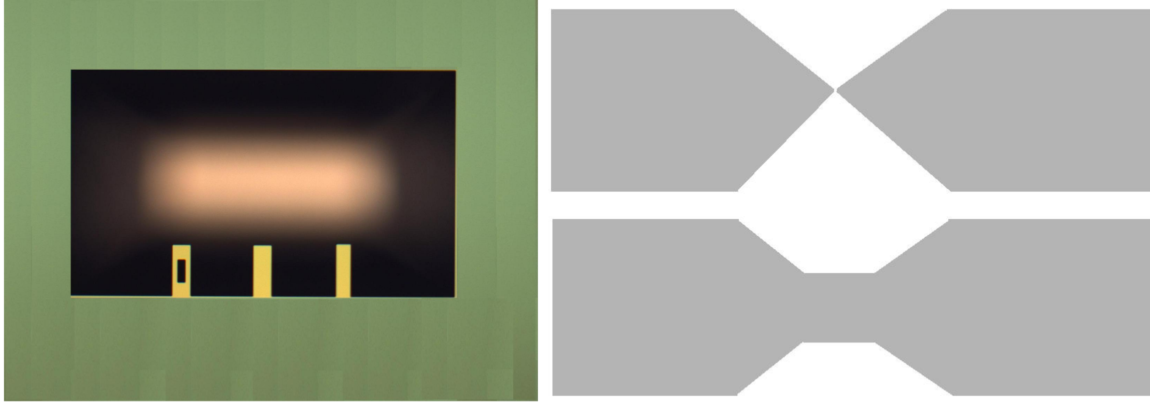

(a) Picture of an under etched region. The bright spot in the middle of the image is the light reflecting on the silicon from the microscope.

(b) Sketch of a side view of an under etched process. The top one is a normally etched silicon, whereas the bottom is an under etched silicon piece.

Figure 5–2: Visual explanation of over etching

5.2 Cantilever Robustness in Water

The cantilevers' fragility and yield due to capillary forces was an issue whenever manipulation in liquid, from the final steps of the TMAH etching to the final immersion in liquid during measurements. This section will focus on the last part where different techniques where used to optimize the outcome of each cantilever.

We originally immersed the cantilevers slowly by filling the bottom cavity of the holder, see fig 6–1(a), until the entire measurement chamber was filled and sealed it, hence avoiding direct contact with the fragile cantilevers and the flow of water. Since we already had evaluated every cantilever prior to the immersion, we were then able to compare the yield ratio of this technique. After several immersions and dry measurements we concluded that, surprisingly, the cantilevers are quite robust if prepared this way. After six immersions of a specific set of cantilevers, only four out

of the 72 cantilevers were broken, giving a 94% yield for this step. The major issue that arose from the submerging did not come from the fragility of the cantilevers but from the immersion technique itself.

We realized that some cantilevers were not completely immersed once the holder was completely full of liquid and sealed. Figures 5–3 show a result when none of the cantilevers are completely immersed in the liquid. The bottom cantilever is in the

Figure 5–3: A photographic image of partly immersed cantilevers

plane of focus and in the liquid, but the two other cantilevers, originally exactly at the same location as the bottom one, are out of focus, or not in the liquid. We realized that because some regions on the cantilevers are not completely etched (see section 5.1), filling the holder from the bottom may not fill all regions. We therefore decided to first delicately deposit a layer of liquid directly on the die. Once the die was covered completely, we waited for one minute and then gently shook the holder

for thirty seconds and let it stand for another minute. We then once again slowly filled the cavity from the bottom until it was full. This experiment was conducted four times with an average improvement of $(9 \pm 2)\%$ between the two techniques. This improvement was significant enough to make it part of the standard procedure for all liquid measurements.

5.3 Bubbles

Another issue that arose when filling the chamber with water was bubbles. It is easy to understand that a bubble bigger than a few microns, if attached to a cantilever, will greatly affect the LASER reflecting on the surface. A protocol was therefore created with the help of Dr. Helene Bourque, a research associate in our group. The only water used was Milli-Q water, water that has been purified and deionized to a high degree by a water purification systems manufactured by a company called *Millipore Corporation*. This water was then poured in a beaker and inserted in an ultrasonic bath for 30 minutes at room temperature. Sonication helps nucleate bubbles and thus depletes the liquid of dissolved gas. A $20ml$ syringe was then used to slowly transfer the liquid from the beaker to the holder's cavity.

5.4 SEM Imaging

As can be seen from equation 2.11, dimensions of a cantilever are critical to evaluate the proper theoretical resonance frequency. We therefore evaluated the dimensions of the cantilever experimentally after the cantilever damping was characterized. This was done to ensure that the discrepancies between the theory and the experiment were not caused by major differences in size. We had no difficulty in evaluating the length nor the width of the lever as any decent optical microscope was

able to provide reasonable resolution, but for the thickness we had to use a scanning electron microscope (SEM). In order to evaluate the data consistently, we decided to measure all of the dimensions with the SEM.

We proceed to evaluate the thickness of the cantilevers using images such as the one shown in figure 5–4.

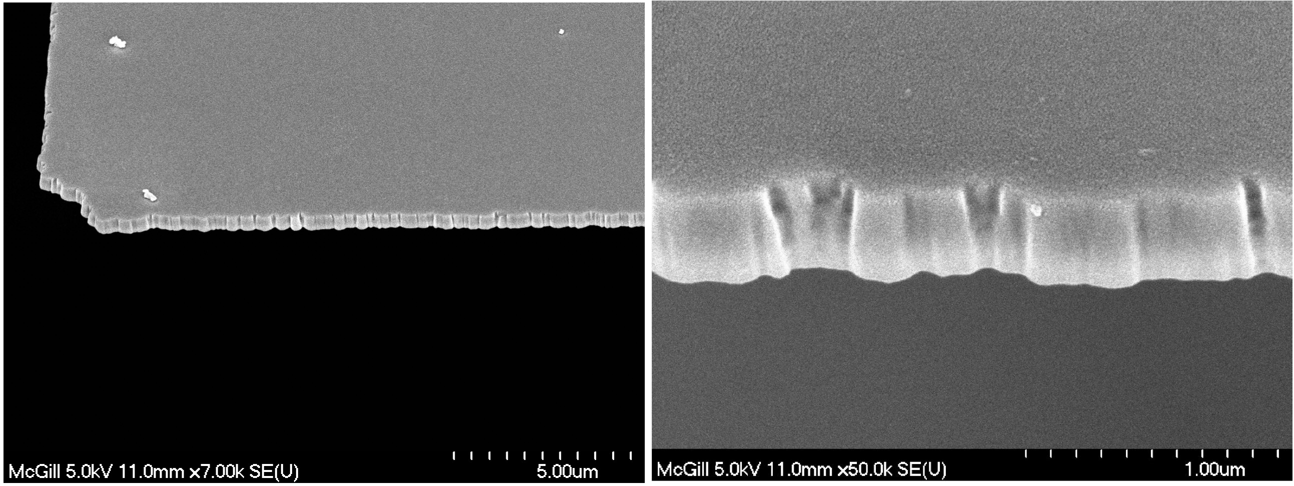

(a) Side view of a cantilever at 40° angle

(b) Close up of another cantilever

Figure 5–4: SEM images of microfabricated silicon nitride cantilevers

A series of images was then gathered at similar magnification as that shown in figure 5–4(b), in order to evaluate the true thickness of the silicon nitride cantilever. This gave $(480 \pm 10)nm$, a difference of 4% from the original $5000\mathring{A}$. It is important to notice that these images were taken at an angle of 40° and the distance measured was therefore corrected for this tilt. The thickness was also evaluated using an ellipsometry and gave a similar result of $(481 \pm 9)nm$. Ellipsometry is a versatile and powerful optical technique for the investigation of the dielectric properties (complex refractive index or dielectric function) of thin films. The same technique was used

during this process flow to assure a uniform thickness prior to starting a full experiment. It is important to note that the specifications from the wafer supplier state that the LPCVD silicon nitride is expected to be $5000\mathring{A} \pm 5\%$. Even though both the aforemention values are within error, they are lower than the original data collected prior to the first etching process. We therefore think that it is safe to say that one of our etching techniques may have caused a slight decrease in thickness of the Si_3N_4 membrane.

Similar procedures were done on images such as the one shown in figure 5–5.

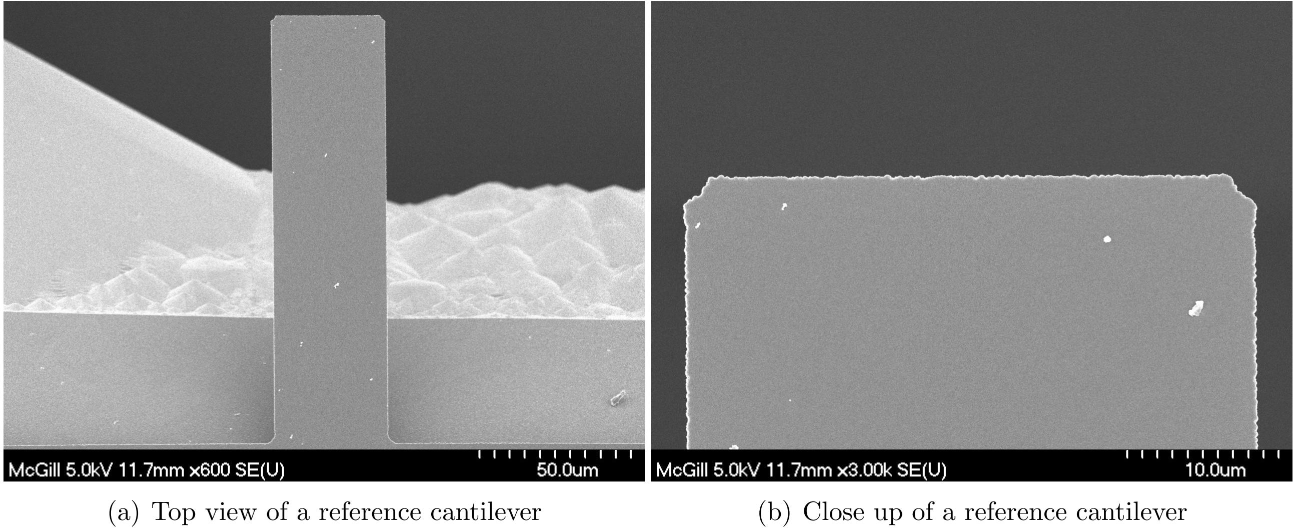

(a) Top view of a reference cantilever (b) Close up of a reference cantilever

Figure 5–5: SEM images of microfabricated silicon nitride cantilevers

Both the width and the height ended up with less than one percent difference with respect to the expected target values. These parameters are therefore not relevant and not considered in the difference between the theory and the experimental value of the resonance frequency.

CHAPTER 6
Experimental Results

This section will focus on the experimental part of this project. We will describe in length the details that make this experiment relevant and reproducible. A great deal of care was taken to ensure the accuracy of the experiments and is described in the next sections.

6.1 Experimental apparatus

The apparatus was originally constructed by Duan Xuefeng, a former member of the group. However, it had to be later modified to decrease the resonance of the setup and to increase the detection bandwidth and stability. The first step was to replace the hollow aluminum base for a solid one. This action improved significantly the stability of the laser-holding base as well as reduced the vibration caused by the surroundings. We also made sure to add extra layers of solid gel between the table and the aluminum slab holding the entire setup. The last major improvement made on the setup comes from the photo diode holder. The L-shape aluminum holder had an obvious resonance frequency and was hindering accurate data collection. We therefore had to add a solid triangular slab of aluminum to solidify the structure, hence reducing the vibrations.

There are three main components in our setup, as shown in figure 1–1. The first one is a LASER that will be used to measure the deflection. This specific light

source had a wavelength of $635nm$ and a nominal power of $5mW$, the part number from *Coherent* is 0221-700-01.

The second component is the sample holder. This consists of an anodized aluminum base sealed with an o-ring and a glass piece. This part was constructed with enough room underneath it to have a uniform flow of liquid and small enough to hold a microfabricated die with several cantilever islands as described in the previous chapter and shown in figure 6–1. By being able to use a whole die instead of a single chip variability in clamping losses due to the mounting of individual chips is avoided.

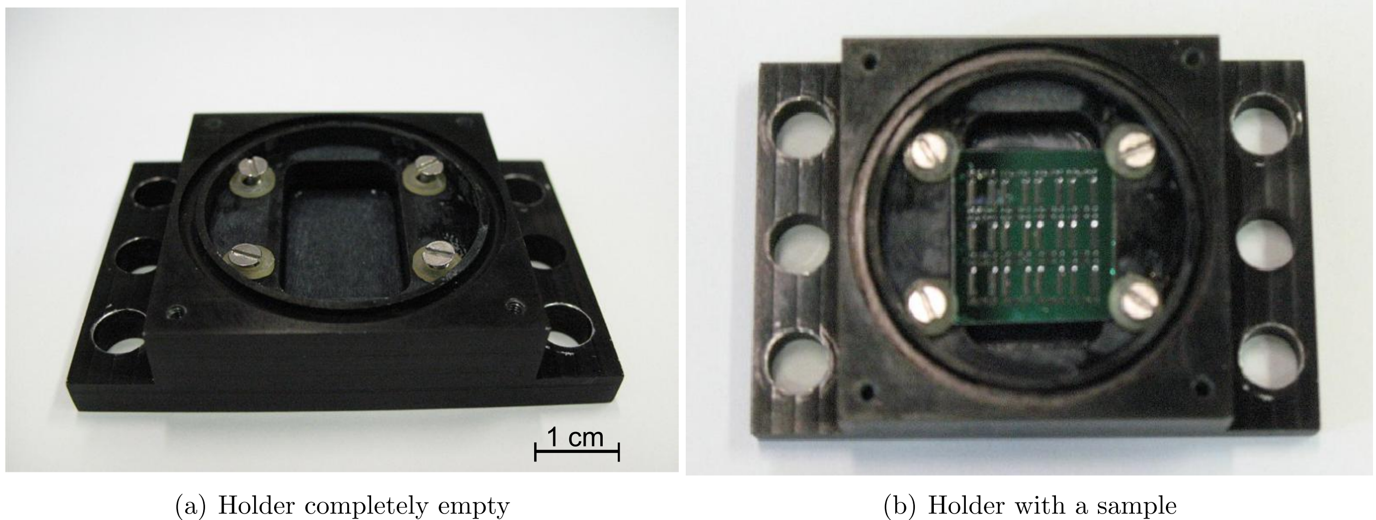

(a) Holder completely empty

(b) Holder with a sample

Figure 6–1: Home made sample holder

The last important component of this setup is the split photodiode that collects the information from the LASER's interaction with the sample. A split photodiode is a split semiconductor diode in which the differential current varies with the respective areas illuminated, hence allowing us to evaluate the position of the reflected beam and

thus deflection of the cantilever. In our case, we used a photodiode from *Hamamatsu* model number $S6695-01$, a diode with an active area of $4mm^2$ and a maximum voltage of $20V$. The entire experimental setup can be seen in figure 6–2.

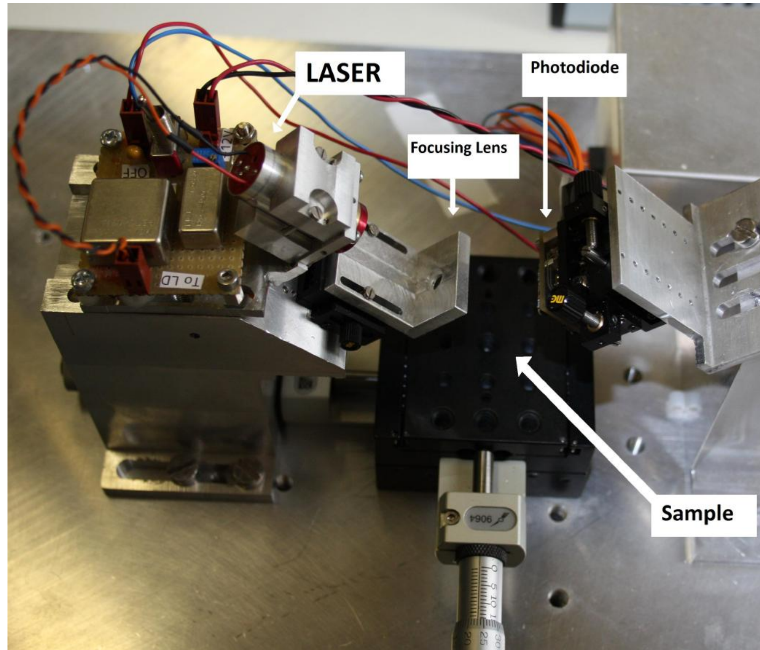

Figure 6–2: Picture of the experimental setup

6.2 Software

All data acquired by the photo diode is collected by an acquisition card made by *Gage Scope Digitizers*. This card is controlled via a LabVIEW program written by Mehdi El Ouali, a graduate student in our group. This acquisition and display program allows you to define many aspects of the acquisition such as number of channels or the type of coupling, but the most important one is the sample rate as explained in section 6.2.1.

All the graphs that you will see in this thesis represent an acquisition that has been converted to make it possible to see information from the data. If the original information were simply plotted without any numerical filtering, the data would simply look like a wide-band noise, as this is what we are measuring, and no valuable information would be easily recognizable. Essentially, we use MatLab code to filter and calculate a power spectral density using the method called fast fourier transform (FFT) of our data. This allows us to measure the fundamental and first harmonic thermal resonance peak of the cantilever. The code used is based on a program created by Mehdi El Ouali, but had to be modified to fit our specific needs.

The information is first modified by *myGDFRead.m*, which reads the data file header containing critical information on how to interpret the data in the file. These parameters are put into a data structure (MatLab struct) called myGDF. The most important parameters are the sampling rates, the number of points and records to read. This allows myGDFReader to determine whether the data is saved in float64 (8 byte floating point number) or in int16 (2 byte signed integer).

This modified data then undergoes a 1-Sided Power Spectral Density (PSD). A PSD shows the strength of the variations as a function of frequency. In other words, it shows at which frequencies variations are strong and at which frequencies variations are weak. In our case, this transforms the data that appeared as simple noise into useful information. The unit of PSD is energy per frequency and its computation is done directly by FFT.

Obviously, this will display all frequency information including that which is not related to the cantilever itself, for example from mechanical vibrations (e.g.

coupling from the building) or electrical noise. These are almost standard in our lab as most people work with very precise measurements. We therefore had a lot of help in understanding their meaning and how to disregard irrelevant peaks during data analysis.

6.2.1 Anti-Aliasing

The default value of the software's sample rate was 1 MHz. The experiment was yielding results well predicted with theory for the first mode of cantilever response, but somehow was giving illogical results for the other modes. It was clear that the card was exhibiting aliasing for this specific sample rate. As mentioned in Digital Systems Reference Book, from B.Holdsworth et al.[27],"it is necessary to remove all frequencies equal to or greater than half the sampling frequency from the input signal. This prevents the aliasing of frequency components into the desired passband from outside due to the modulating effect of the sampling process "[27]. A definition clearly explaining our situation where our prior choice of sample rate was interacting with the low pass filter. We therefore changed the sample rate to 10MHz and re-evaluated the same cantilever to compare the two methods. The red and green line on figure 6–3 shows the results of two independent readings of a specific cantilever performed with a sampling rate of 1MHz and 10MHz.

As can be seen from the figure, the location of the first mode at approximately 30kHz is identical, independent of the sampling frequency. A peak at 100kHz is clearly visible on the blue and red curves but does not match any of the theoretical calculations for this cantilever. There is a third peak, located a little before 200kHz, that does agree with theoretical estimates and is present for the three curves. The

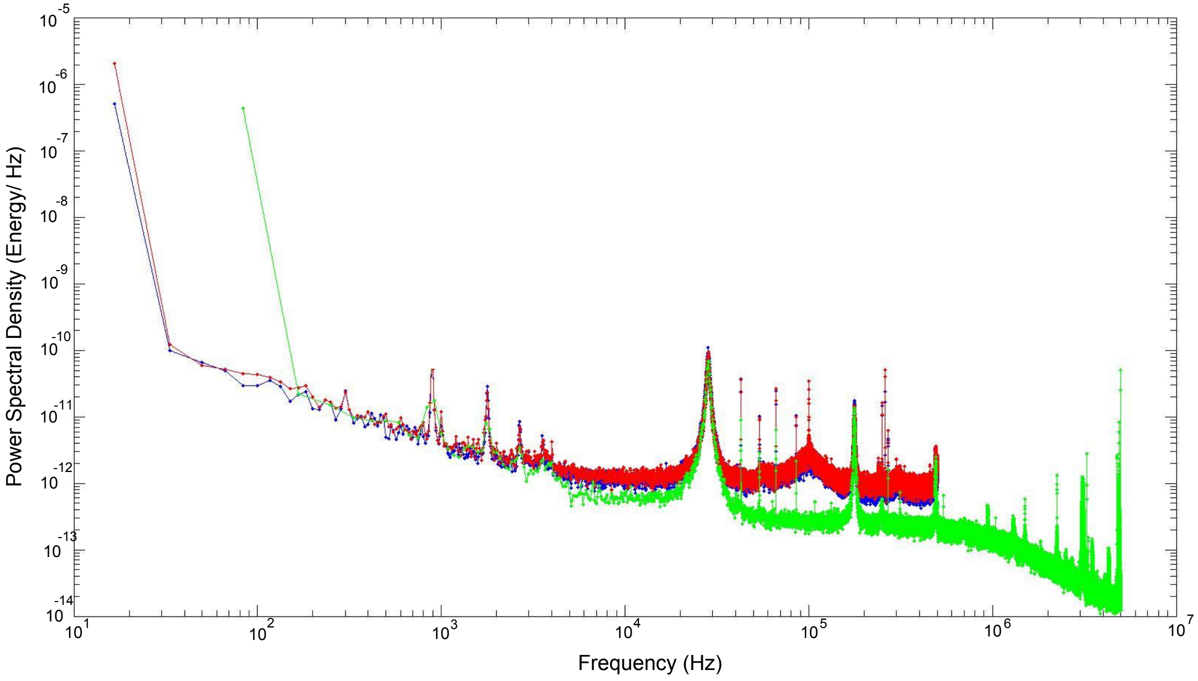

Figure 6–3: Effect of aliasing. X axis is Hz. Y axis is a normalized arbitrary unit of intensity. Blue and red were collected at 1MHz and the green at 10MHz

biggest relief from the switching to 10MHz results was the low pass filter behavior at 1MHz and the clear lowering of the base line throughout the measurements. This roll off was expected at this value as it matches with the photodiode bandwidth. This modification assured us that proper peaks were not getting buried in noise and aliasing was not introducing artifacts.

6.2.2 Laser Position

It was showed by Fuchs et al. that the location of the laser on a cantilever may have an unexpected effect on measurments[28]. If a cantilever is bigger than the LASER spot size (relevant for the present work), the location of the beam may

coincide with a mode node and could cancel out its contribution, as pointed out by the red arrows of figure 2–1. This effect, as can be seen from the same figure, does not interfere for the first mode, as there are no nodes, but could do so on subsequent ones and alter the data sets. A consequence of this effect was observed on many occasions, and a typical outcome is shown in figures 6–4 and 6–5.

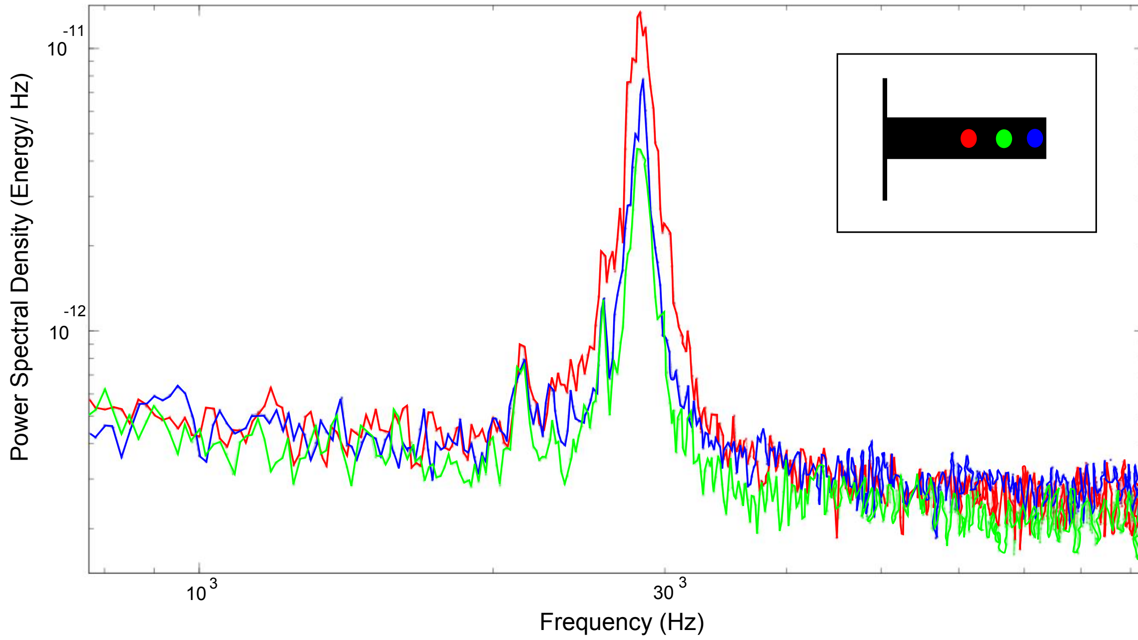

Figure 6–4: 1st mode of a base cantilever($\approx 28kHz$).The 3 colors represent different locations of the laser beam on the lever. Inset is a representation of the laser position on a cantilever.

The two figures are taken from the same cantilever. The three lines represent different readings at different positions of the LASER on the cantilever. The blue line was aimed at the free end, the red line in the middle of the cantilever and the green line in between the two. You can clearly see from the image that the second mode

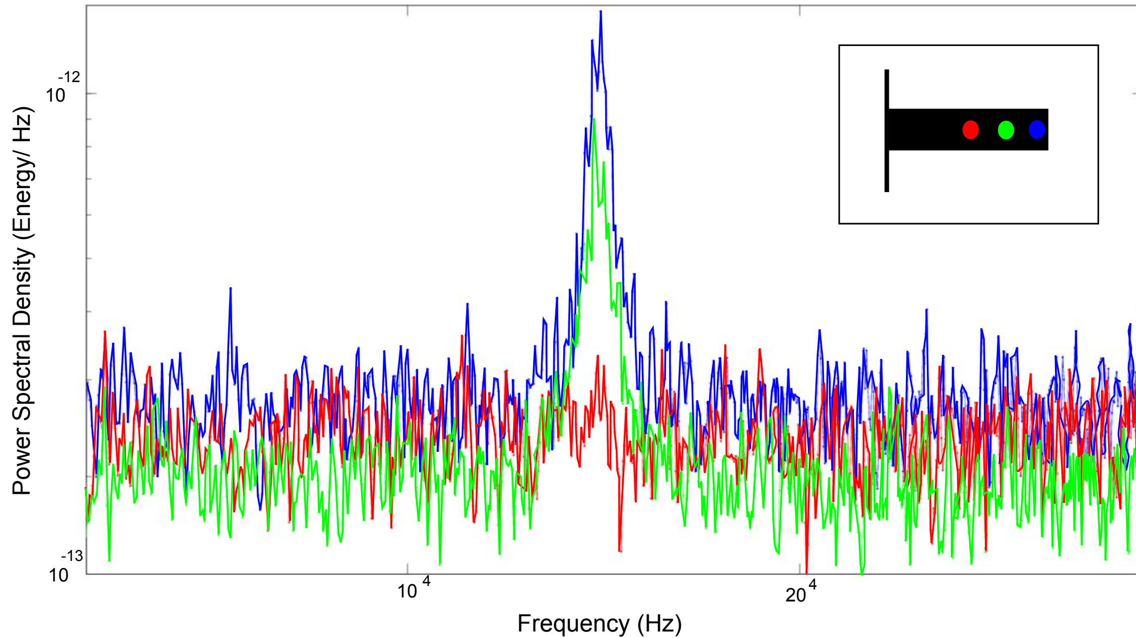

Figure 6–5: 2nd mode of a base cantilever($\approx 177kHz$). Same as above except that the second mode of the red line disappeared.

of the red line disappeared, probably due the concept explained above taken from Fuchs et al.[28]. After several trials, we realized that the green line was redundant and was always giving the same response as either the red or the blue line. For that reason we have decided that for every single cantilever we would take two individual measurements; one in the center and one on the tip. They can be differentiated using C or a T as the last letter of an original data set.

6.3 Results

All cantilever measurements were done on the apparatus presented in section 6.1 and were all analyzed using the software explained in section 6.2. Once a peak was identified as a potential mode, a fit of the data was executed using a Lorentz

distribution and data was collected. The resonance frequency was taken directly from the fit and the quality factor of each peak was evaluated using equation 2.9. The instances where both peaks were present (see section 6.2.2), an average of the two were taken as the data of this cantilever and when only one peak was present information from the fit was taken as is.

6.3.1 Resonance Frequency and Quality Factor

The first set of results is shown in table 6–1 and represents the value for all the reference cantilevers measured in air compiled together.

Measurement in Air			
Mode	Experimental (kHz)	Theoretical (kHz)	Q-Factor
1	28.3 ± 0.2	37.6	22 ± 6
2	177.0 ± 0.8	236	90 ± 10
3	491 ± 3	661	150 ± 40

Table 6–1: Values for the reference cantilever in air

After a thorough investigation it was concluded that the expected theoretical values calculated using equation 2.10 with E=290GPa, the average of values quoted in literature [29], and experimentally determined dimensions do not match the experimental data. More than 200 cantilevers were measured to obtain these values. One interesting aspect is the fact that all the theoretical values are almost exactly 25% less than the theoretical one (25.1 ± 0.5), which suggests that the difference between the two may be a specific parameter, the result of particularly uniform cantilevers due to careful processing. For this reason we can assume that one of the parameter was not properly defined and since the only parameter we could not control or evaluate

was the Young's modulus, we will assume that the value of $290GPa$ used was erroneous and we then used $190GPa$, a value in the lower range quoted in the literature of $190 - 385GPa$ [30]. Using $E = 190GPa$ we now obtain an excellent agreement between the measured and theoretically expected values. The same previous data would then look like this:

Measurement in Air			
Mode	Experimental (kHz)	Theoretical (kHz)	Q-Factor
1	28.3 ± 0.2	29.1	22 ± 6
2	177.0 ± 0.8	181	90 ± 10
3	491 ± 3	501	150 ± 40

Table 6–2: Values for the reference cantilever in air with an assumed Young's modulus of 190 GPa.

This experimental data now agrees with the theoretically expected resonant frequency to within 2%. This, as well as the small experimental variation, demonstrates that we have achieved excellent process control and reproducibility. Table 6–3 was collected the same way as the previous one except that every cantilever was completely immersed in water.

Measurement in Water			
Mode	Experimental (kHz)	Theoretical (kHz)	Q-Factor
1	4.3 ± 0.1	5.9	2.0 ± 0.5
2	35.2 ± 0.3	46	4.8 ± 1.5
3	109 ± 1	124	7.5 ± 0.9

Table 6–3: Values for the reference cantilever in water

The discrepancy between experimental and expected theoretical values using equation 2.11 is now approximately 10-20%, well above the experimental uncertainly and variability. This brings to question the fundamental validity of equation 2.11 for

cantilevers immersed in water, that seem to give better results in fluid with lesser density.

The same kind of experiment was repeated but this time with the cantilevers of interest. Obviously we do not have as much statistics on these, simply because we have less levers per wafer to evaluate. Cantilevers 1 to 12 are the number representation of each of the different cantilevers as shown in the sketch of figure 4–2 and 4–3, and the results can be observed in table 6–4 and 6–5. Notice that only two modes were recorded in these two tables and the reason is that for too many cantilevers the third mode was not observable, especially in water.

Modified Cantilevers in Air				
Cantilever	1st mode(kHz)	Q-Factor (±0.7)	2nd mode(kHz)	Q-Factor (±0.8)
1	30	26	183	68
2	18	17	134	30
3	21	21	127	58
4	29	28	168	90
5	27	27	177	66
6	26	22	174	63
7	29	24	188	54
8	30	21	189	70
9	28	32	195	89
10	28	28	194	70
11	27	18	174	51
12	25	13	209	63

Table 6–4: Values for the modified cantilevers in air

The information from these tables are not as clear as it was in the previous tables. One thing is certain is that there are no significant improvement within individual cantilevers' Q-factor if compared to the reference lever. Some cantilevers (2,11 & 12) did however demonstrate a more pronounced reduction in quality factor than

Modified Cantilevers in Water				
Cantilever	1st mode(kHz)	Q-Factor (± 0.8)	2nd mode(kHz)	Q-Factor (± 0.8)
1	4.3	1	44	1
2	2.0	1	31	1
3	2.8	1	41	1
4	4.1	1.5	40	3
5	4.1	2	40	3
6	3.5	1.5	40	2.5
7	4.5	2	37	4
8	4.5	2	37	5
9	4.0	2	38	5
10	4.3	2	38	4
11	3.7	1	39	2
12	3.3	2	37	1

Table 6–5: Values for the modified cantilevers in water

the others. Cantilever 4 and 9 showed the most interesting features. These two cantilevers have shown the most evidential improvement from the rest of the designs, mainly apparent in their second mode. This statement is valid in both water and air and leaves it at par with the reference cantilever. These specific models (2,4,9,11& 12) should be the premise of future work on the subject in order to surpass the reference cantilever.

Because the tabulation format makes it hard to compare and draw empirical conclusions, we have made a plot that enhances another aspect of this data set. In figure 6–6 & 6–7 we show the quality factor by mode. On each graph 4 lines can be observed. The top line is the value of each cantilevers' Q-factor in air. The bottom one is the same value but this time in water. The blue line is the ratio line, it represents the percentage value of the quality factor in water over the one in air. This ratio line is important, as a strong reduction shows a strong influence of the

effect of the medium. The dotted line is the experimental value of that same ratio but for the square reference cantilever. The grey area is the error attached to this same line.

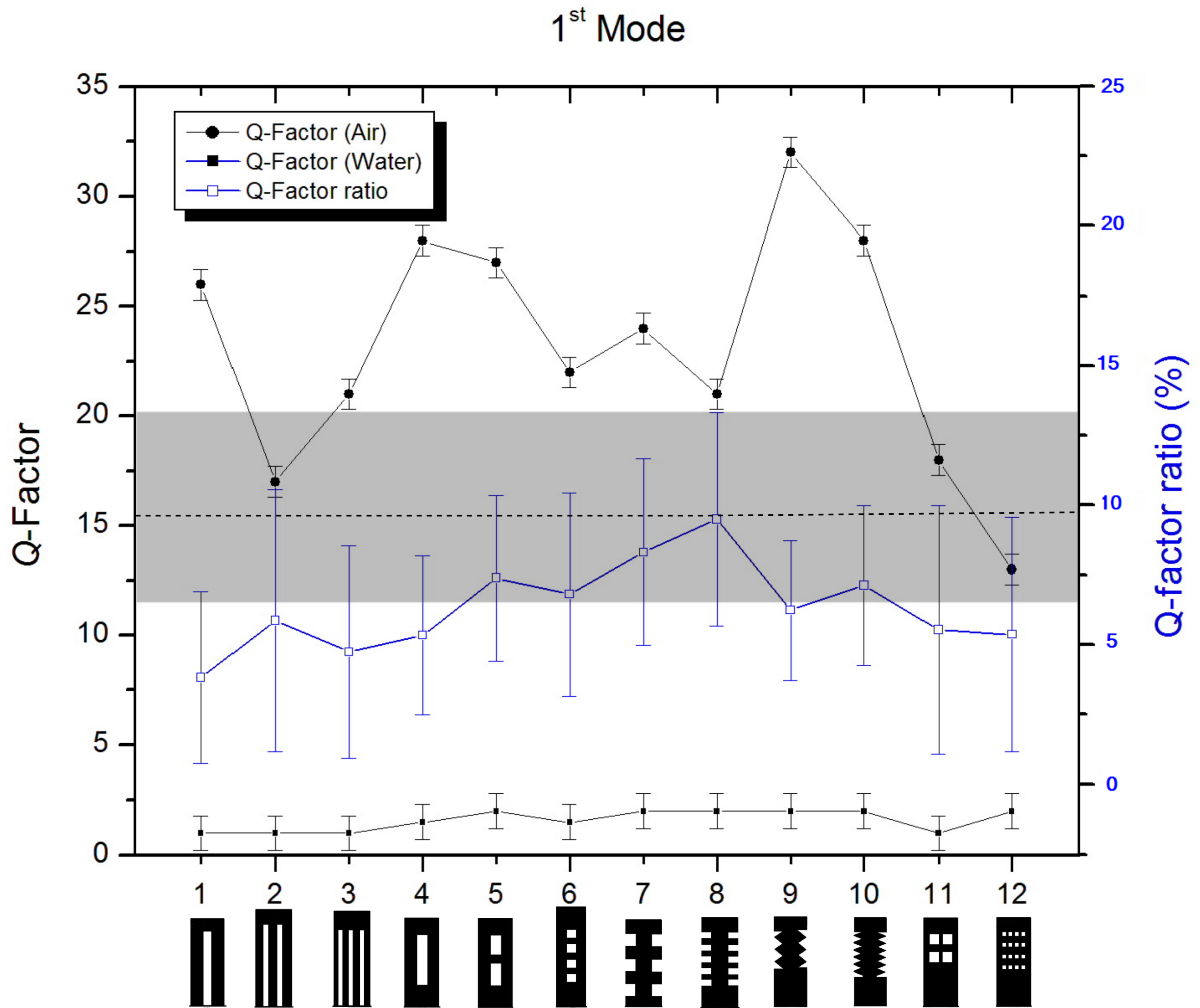

Figure 6–6: 1st mode Q-factor and ratio. Top line is the Q-factor in air. The bottom line is the Q-factor in water. The middle line that uses the right y-axis is the ratio of Q-water over Q-Air. The dotted line is the same ratio but for the reference cantilever, and the grey area is the error attached to that number.

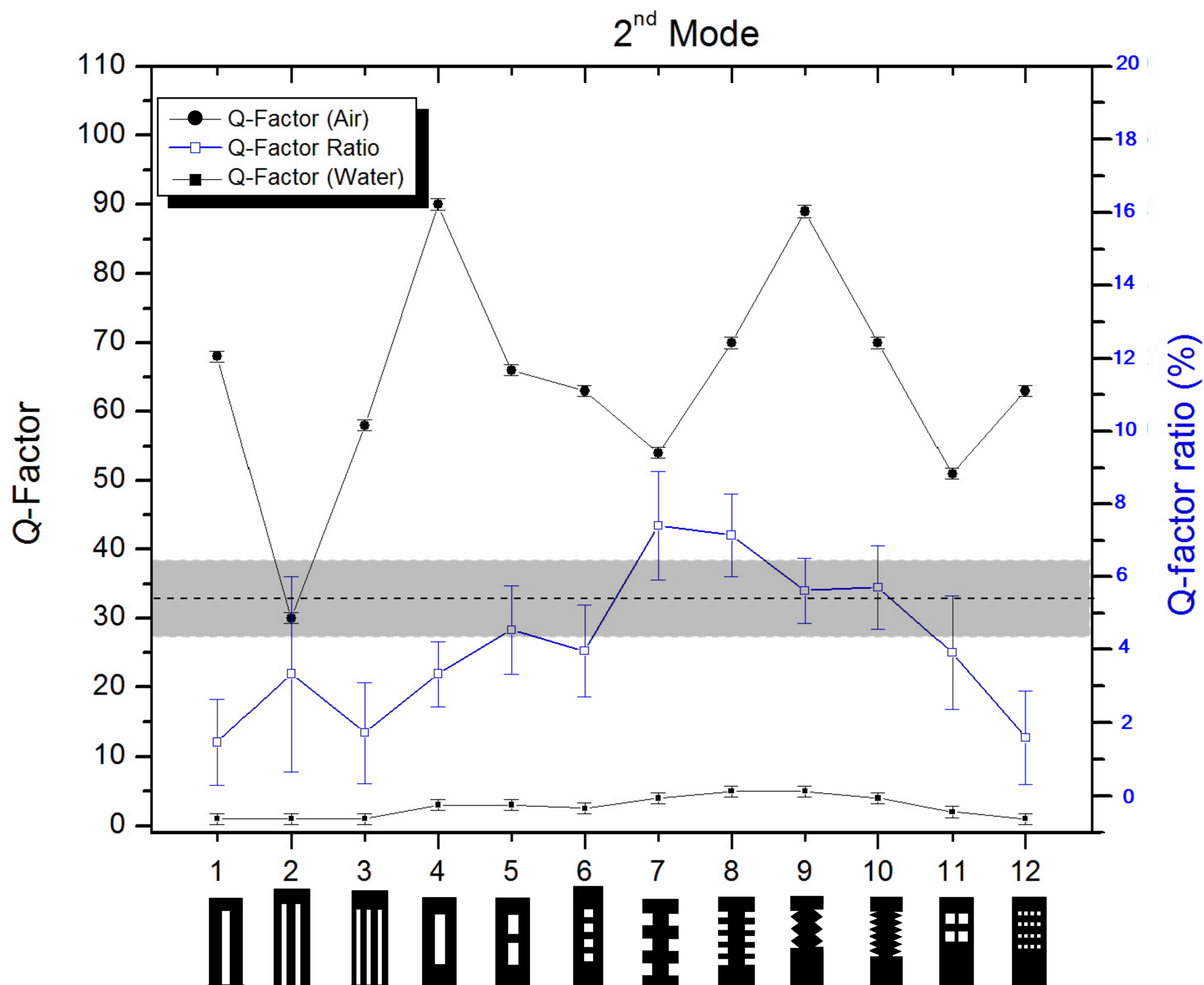

Figure 6–7: 2nd mode Q-factor and ratio. Top line is the Q-factor in air. The bottom line is the Q-factor in water. The middle line that uses the right y-axis is the ratio of Q-water over Q-Air. The dotted line is the same ratio but for the reference cantilever, and the grey area is the error attached to that number.

In this first graph we clearly see the low peaks in air mentioned above, namely 2,11 and 12, as well as the two main apexes in 4 and 9. The dotted line and the

grey area are at 9 ± 3 and represents the ratio for the reference cantilever. The ratio allows the identification of promising structures that should be further investigated.

In the second graph the dotted line is at 5 ± 2 and the apexes are at the same place in the 1st mode. In this graph however four cantilevers seems to have a higher ratio than the reference one, 7, 8, 9 and 10. One, however, has to be careful not to draw conclusions too quickly as the ratio calculated is highly affected by the value of the quality factor in air. Since cantilever 9 is the only one with a resonance frequency similar to the reference cantilever in air and a slightly higher one in water, this lever comes up on top for this graph. One conclusion that can be drawn from these graphs is that in the first mode no cantilevers show a significant improvement over the reference one. In the seconde mode, however, cantilever number 9 made a very small improvement over the reference one, clearly distancing itself from the others. One very interesting point to also gather from these two tables is the fact that cantilever 7,8,9,10 showed an improved behavior compared to the others. Going back to table 4–1 it is clear that, along with cantilever 4, these are the cantilevers with the least amount of surface contour hence interface with the fluid. The reason why cantilever 9 is found to be ideal in this case could then be a composition of design and an optimization of the ideal contour size. Both aspects are legitimate claims and should be pursued further.

Another aspect that we found useful to look at is the behavior of the resonance frequency with respect to the quality factor. We therefore created figure 6–8 to promote this relationship.

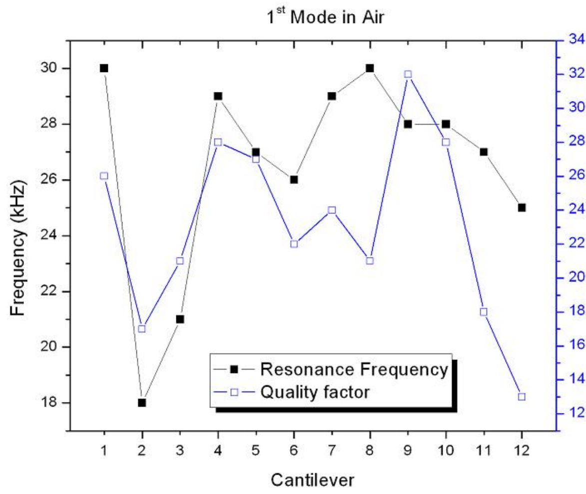

(a) 1st mode's resonance frequency and quality factor in air. Cantilever 4 and 9 are slightly above, whereas 2 and 12 bellow.

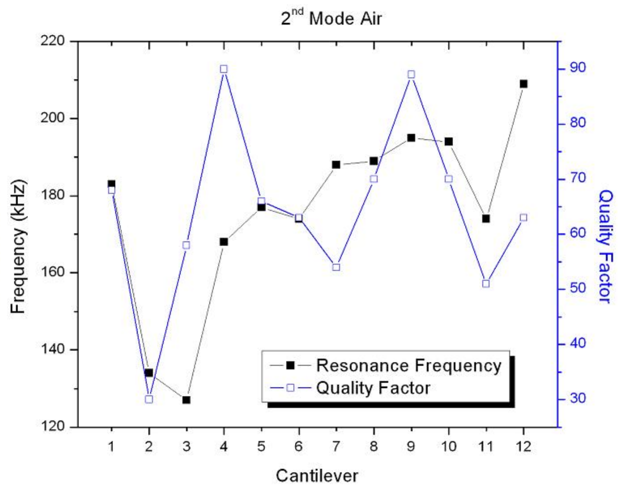

(b) 2nd mode's resonance frequency and quality factor in air. Cantilever 4 and 9 are above the normal path.

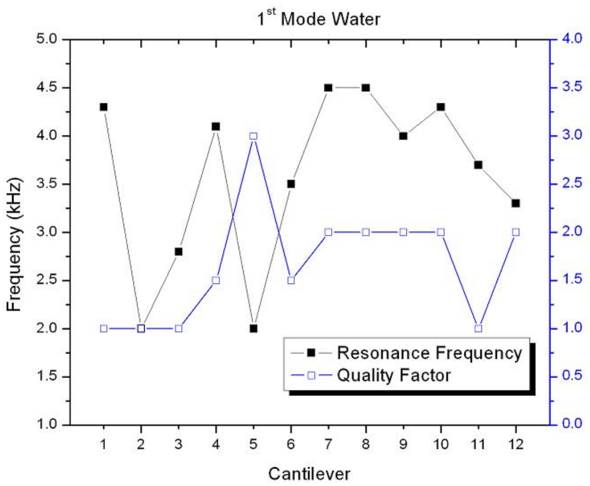

(c) 1st mode's resonance frequency and quality factor in water. This is the only time cantilever 5 showed any interest. Error in the data collection of this cantilever has to be considered.

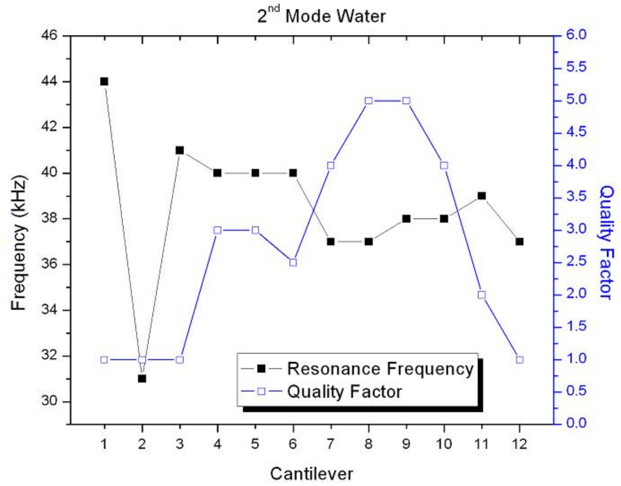

(d) 2nd mode's resonance frequency and quality factor in water. Cantilever 7, 8 and 9 are once again above the usual pack.

Figure 6–8: Comparison between resonance frequency behavior and quality factor in both air and water for both modes.

The general idea to take out of these figures is that there is a correlation or pattern for the resonances and the Q-factor, except for the cantilevers of greater interest. This indicates that often equation 2.9 and 2.11's are reasonably accurate descriptions, even if some cantilever designs are clearly setting themselves apart from the pack. These specific cantilevers are the same ones as observed in the previous analysis, but would require additional measurements in order to further extend this hypothesis.

The last aspect that had to be measured was the difference between the cantilever of interest and the middle cantilever. This analysis will ensure that the different shapes of each cantilever of interest are actually making a difference in the resonance frequency and the Q-factor not only due to the overall change in outside contour dimensions. Table 6–6 shows the outcome of this comparison.

Reference versus modified cantilever		
Cantilever	Air (%)	Water (%)
1	-11±8	-12±5
2	-29±1	-39±2
3	-19±9	-17.7±0.5
4	-6±3	-6±2
5	5±2	0.9±1.1
6	-19±4	-19±4
7	-15±4	-9±2
8	12±2	12±5
9	-14±3	7±3
10	-29±2	10±3
11	5±1	-2±1
12	6±2	0.1±1.6

Table 6–6: Difference between reference and modified cantilever. The two cantilevers have the same contour dimension. The reference one is a simple rectangular cantilever whereas the modified one has special features. A negative number signifies that the resonance frequency on the modified cantilever is smaller than the reference one.

It is clear from this table that most cantilevers do show a clear difference between the two, which brings us to believe that the features from the reference cantilevers are actually making a difference and not only the change in overall contour dimensions. There is, however, some exception coming once again from cantilevesr 11 and 12. They are the only two levers (along with 5) that have expressed a greater resonance frequency in air and an extremely low difference in water, pushing the idea that these models should be regarded as very interesting when future work is pursued on the subject.

6.3.2 Cantilever Contour

The contours of the cantilevers are bound to affect their behavior in fluid. Whether the interaction of the laminar flow with the new boundary conditions created by the extra edges will enhance the quality factor or the other way around still had to be shown. We, therefore, constructed a comparison plot with the contour length and the quality factor's 2nd mode, shown in figure 6–9.

A clear trend is obvious at first glance from this plot. The quality factor seems to be directly proportional to the inverse of the contour length. As expected, the more edges a cantilever has the more turbulence in the fluid it will create. This increase of turbulence turns out to be directly related to the performance of the quality factor. This concept is very clear and should be elaborated more in subsequent investigation.

6.3.3 Cantilevers Interference

Another aspect of the cantilevers' arrangement was made to evaluate whether or not there was any coupling between neighboring cantilevers. The spacing of $170\mu m$,

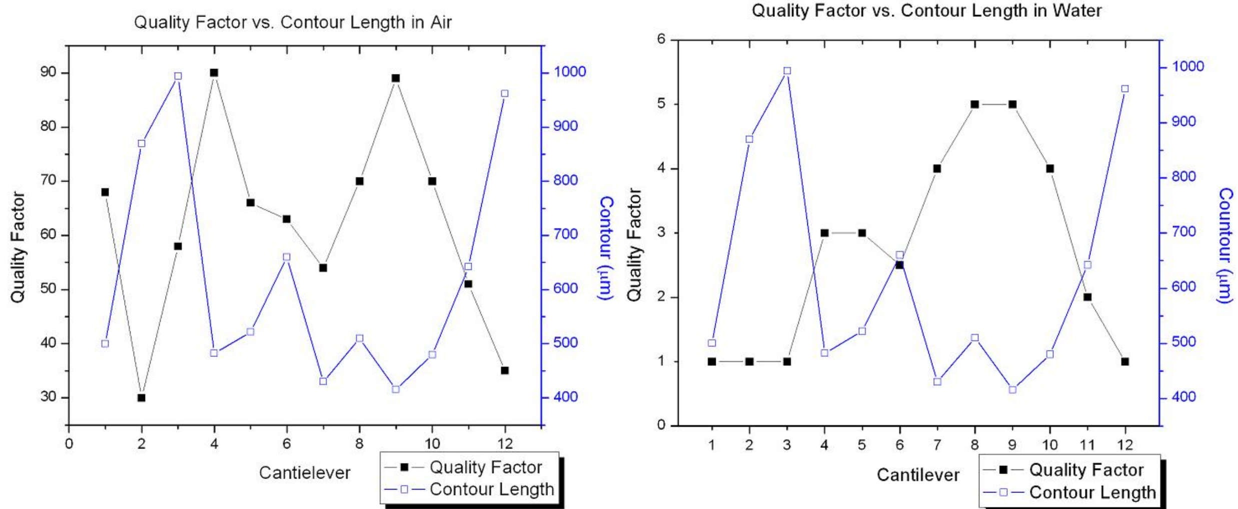

(a) Second mode quality factor versus contour length in air.

(b) Second mode quality factor versus contour length in water.

Figure 6–9: Comparison between quality factor and contour length in both air and water for the second mode.

for the top cantilevers, was chosen to make the most uniform repetition of the cantilevers and the box surrounding it. This size of the box was originally used by Duan Xuefeng in his masters thesis[17], where the coupling issues between the levers where not addressed. We therefore assumed that there would be no difference between the two measurements. As one can see from table 6–7 this assumption was erroneous.

Differences Between Top and Bottom Cantilevers				
	1st Mode		2nd Mode	
Merdium	Resonance (Hz)	Q-factor	Resonance (Hz)	Q-factor
Air	+307 (1.1%)	+1.3 (6%)	+1750 (1.0%)	+1.7 (2%)
Water	+291 (6.7%)	+0.2 (10%)	+2700 (7.6%)	+0.4 (4%)

Table 6–7: Difference between top and bottom matching cantilevers. This difference is calculated to ensure there is no coupling within neighboring cantilevers.

The numbers may look small percentage-wise, but it is interesting to note the fact that all the values are positive and increase with the viscosity of the coupling medium. To calculate this data, we gathered all the base cantilevers on all the die and paired them up with their respective neighbors on each island. The resonance frequency on the top cantilever was subtracted from the bottom cantilever and added to the data set, to be then divided by the number of pairs. This techniques should theoretically give zero for perfectly identical cantilevers, or at least a succession of small positive and negative numbers that would eventually, with much more data, approach zero. We instead obtained only positive numbers with a very small standard deviation of $7kHz$ or 2.3% for the first mode and 2.1% for the second one.

We did however expect that if coupling was observed between adjacent cantilevers, it should be significantly greater in water than in air as table 6–7 corroborates. This assumption was based on basic fluid dynamics and backed up by a paper by J.N. Newman[31] which explained the propagating behavior of water from rigid surfaces.

CHAPTER 7
Conclusions and Outlook

Throughout this work the reader was carried through the steps required in the elaboration of a plan to improve the quality factor of an immersed cantilever. From the conception of the different cantilevers to the measurements in our house built apparatus, all the details have been laid out for the reader to understand and reproduce this experiment.

We started by giving a concise the introduction of atomic force microscope and its different modes of operation. With this technology came the concept of resonance frequency as well as the quality factor. Both of these notions turned out to be the key aspect of this work and were investigated during the duration of the project.

We then moved on to a step by step method to produce the cantilevers in the clean room here at the *McGill Nonotools-Microfab*. From the fabrication of the masks and the reasoning behind the specific selection of the cantilevers, to the specifics of all apparatuses used during a complete process flow. Details were given to ensure that a potential new student working on the continuation of this project could reproduce the results straightforwardly. The microfabrication learning curve turns out to be the most time consuming portion of this project and although we had a great deal of help form the supporting staff, time is precious in a clean room environment and can slip away very quickly if not properly guided in the meander of the details.

We also added a section geared toward the issues that arose during the experiment, from the production of cantilevers to the measurement of these same levers. The primary purpose was once again to educate the reader on how to avoid getting similar issues that we encountered and go about producing stable and consistent results.

For the result section of this report we started by explaining the home made experimental apparatus used for the project, an instrument that had to be modified to better suit our needs. We continued this section by explaining the software that was collecting the data from the photodiode as well as some issues that arose with the position of the laser spot on the cantilever. Both the resonance frequency and the quality factor of each cantilever were carefully measured in two different medium, mainly air and pure deionized water. It was shown in this section that the different shapes do affect the Q-factor, but none of them showed significant improvement, although some greatly decreased it clearly minimizing the contour length maximize Q-factor (or minimizes dissipation). A future project might attempt to "lubricate" the edges, e.g. by using a self assembled monolayer of fluorinated molecules. In addition, micromachining leading to very smooth edges (see waviness of edge in SEM figure 5–4(b)) might be worthwhile to pursue. Some specific shapes were targeted to be the most obvious track to start continuing work on the subject. The other aspect we wanted to measure was the interference between adjacent cantilevers, due to their proximity. After showing all the collected data for this specific behavior, we noticed a clear trend that increased the resonance frequencies of cantilever closer to each other. We also added two important graphs, one for each mode, that compare

the quality factor of each cantilever in each medium as well as a ratio of the two with respect to the reference cantilever. These two plots alongside the data from the contour area of each lever allowed us to draw conclusions that both the contour and the design of the cantilever was of critical nature to optimize the quality factor of cantilever in non-vacuum environment.

Using an scanning electron microscope we demonstrated that the width and length of the cantilevers were,within error, of the exact designed value; the thickness was however smaller than stated by the manufacturer of the silicon nitride wafers. In order to theoretically describe the resonance frequency of these levers, an elastic modulus in the lower accepted range had to be used. It is also well possible that the etching process could have caused a porosity in the cantilever, hence decreasing its density. We had no means of evaluating the density or the Young's modulus of the Si_3N_4 film here at McGill but specialized tools are available for that purpose.

Overall detail work was presented with a clear goal to identify crucial factors influencing and thus understand and improve the quality factor of cantilevers immersed in fluid. This work was based on the concept that atomic force microscope measurements of living organisms has to be carried out in their natural habitat, usually a liquid, and that in order to achieve results beyond those previously mentioned work, the response of the cantilever had to be improved if this technique were to be successful. In the end, we were able to show which models were definitely not an option for the future as well as specific ones that could be pursued as potential candidate cantilevers to achieve this goal.

Appendix A

Example of CAD drawing of a photolithography mask.

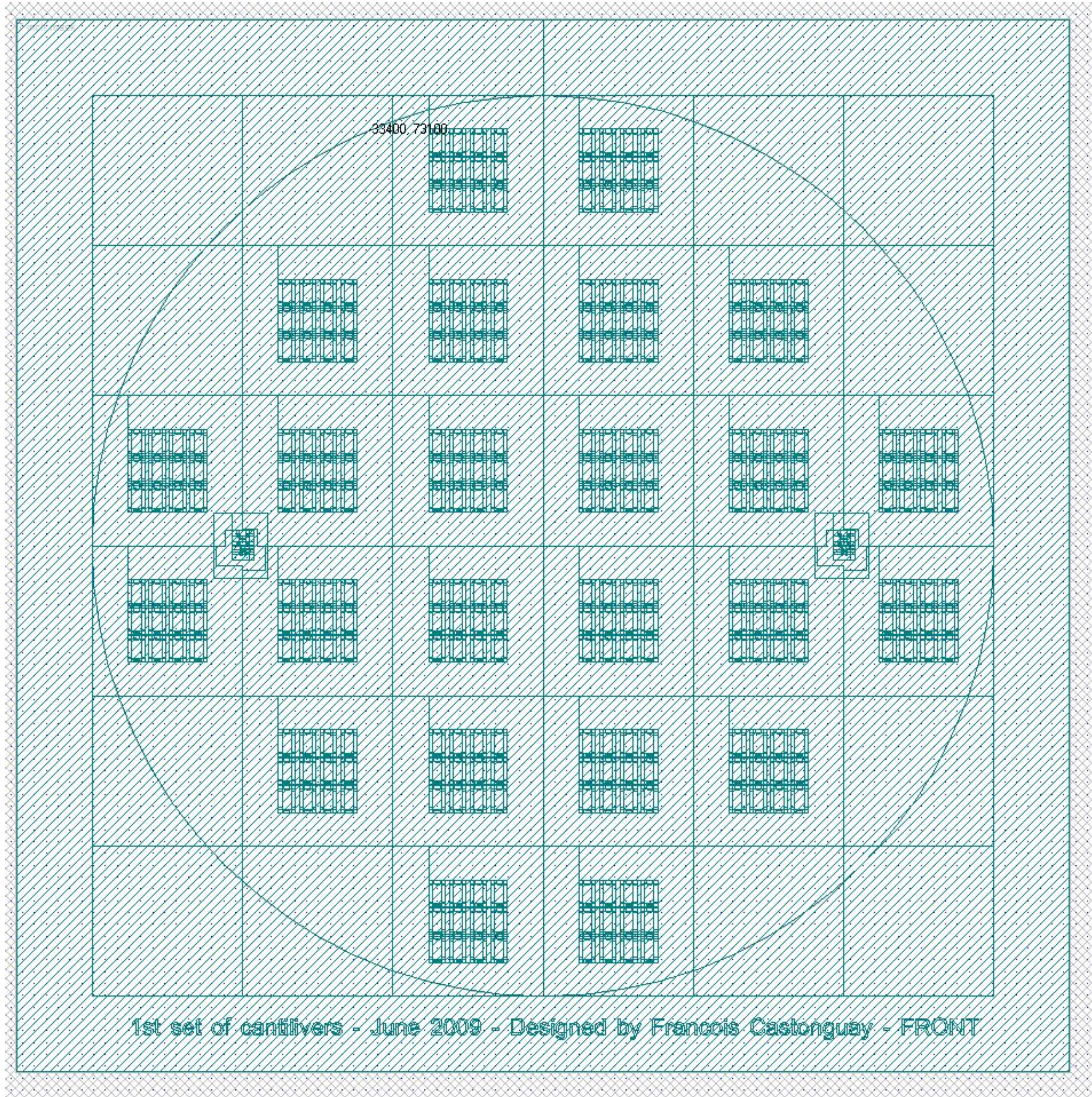

Appendix B

Example of a process flow used for the microfabrication of silicon nitride in a clean room environment.

EXPERIMENTAL PROCESS FLOW

Title: LPCVD Silicon Nitride Cantilever Process Development (using DSP, single SEMI flat, 150mm silicon substrates)

Name: François Castonguay

Date: 09/12/2009 rev.13

Special instructions:

1) Start with prime, clean wafers, straight out of the box. If box has been opened before, check to see whether a clean is advisable.
2) Throughout processing, ONLY handle with clean wafer tweezers. Take care not to scratch the wafer surface and its sides throughout processing.
3) CLEAN equipment process chucks BEFORE loading wafers.
4) NEVER place wafers on ANY surface other than on equipment process chucks.
5) STORE wafers in a closed box when not being processed. Minimize the amount of time that the box is kept open at all times.
6) Track wafer ID via unique laser scribe on each wafer - note the last 3 digits of each scribe on this sheet.

Step	Process Step Name / Description	Comments	Results	Date/Time Completed	Sample/Wafer # 1	2	3	4	5	6	7	8	9	10	11	12
Mask 1	**Front cantilever**															
measurement	Nanospec: Si3N4 thickness	Measure 5 points: top, bottom, left, right, center			X	X	X									
clean	Solvent clean	acetone followed by propanol followed by DI rinse followed by Verteq rinser/dryer			X	X	X									
PR coat	Site: HMDS prime with beaker	recipe: HMDS.In			X	X	X									
	Site: 1.4um S1813 coat & bake (115C)	recipe: 6C14NEBR.In IMPORTANT! No front EBR - must keep Si3N4 on wafer edge intact			X	X	X									
expose M1	EVG: Front alignment, adjust mask thickness to 3.06	Use Bond Chuck with recessed center to minimize wafer to chuck surface contact (exposure: 60mJ/cm2) Mask 3.06mm			X	X	X									
develop	Site: 60sec develop & bake @ 90C	recipe: D1813_60.In			X	X	X									

IMPORTANT! Check Si3N4 etch rate in Applied before next step.

Step	Process Step Name / Description	Comments	Results	Date/Time Completed	1	2	3	4	5	6	7	8	9	10	11	12
etch	Applied: nitride etch (CF4/CHF3)	Etch to silicon (~ 400 sec)			X	X	X									
PR strip	PVA: O2, 60min, 350W, 1mBarr				X	X	X									
inspection	Olympus microscope (10X)	Inspect for residues on entire wafer surface; use "double S" pattern. If residues observed, take necessary corrective action and document here.			X	X	X									
Mask 2	**Back window & break line mask**	M3 used to pattern backside of wafer														
PR coat	Site: HMDS prime with beaker	recipe: HMDS.In			X	X	X									

Step	Process Step Name / Description	Comments	Results	Date/Time Completed	Sample/Wafer #											
					1	2	3	4	5	6	7	8	9	10	11	12
	Site: 1.4um S1813 coat & bake (115C)	recipe: 6C14NEBR.ln IMPORTANT! No front EBR - must keep Si3N4 on wafer edge intact			X	X	X									
align M2 to M1	EVG: Front to back alignment, adjust mask thickness to 3.06	Use Bond Chuck with recessed center to minimize wafer to chuck surface contact (exposure: 60mJ/cm2)			X	X	X									
develop	Site: 45sec develop & bake @ 90C	recipe: D1813_45.ln			X	X	X									
IMPORTANT! Check Si3N4 etch rate in Applied before next step.																
etch	Applied: nitride etch (CF4/CHF3)	Etch to silicon (~400sec)			X	X	X									
PR strip	PVA: O2, 60min, 350W, 1mBarr				X	X	X									
Oxide Dip	Remove deposited ambient layer of oxide	6:1 NH4F:HF ~10 sec			X	X	X									
IMPORTANT! Check TMAH etch rate by evaluating a wafer every hour for the first hour																
bulk Si etch	25% TMAH, fresh solution, 85C	Adjust time to etch 650um of Si so as to leave no silicon . About 23 μm/Hr			X	X	X									
rinse	transfer to rinse bath - soak 10min	DO NOT activate spray! Handle substrates VERY carefully to avoid shattering front features. Keep wafers vertical and GENTLY agitate up and down.			X	X	X									
Oxide etch	Removal of oxide protective layer	6:1 NH4F:HF ~6 min			X	X										
rinse	transfer to rinse bath - soak 10min	DO NOT activate spray! Handle substrates VERY carefully to avoid shattering front features. Keep wafers vertical and GENTLY agitate up and down.			X	X										
Drying	Critical Point Dryer	Follow procedure to dry one wafer at the time														
VERY IMPORTANT! Check for cantilevers quality and then separate in box.																

References

[1] Gerber Ch. Quate C.F. and Binnig G. Atomic force microscope. *Physical Review Letters*, 56:930–933, 1986.

[2] Bowen Richard W. and Hilal N. *Atomic Force Microscopy in Process Engineering.* Elsevier, 2009.

[3] Wiesendanger R. Morita S. and Meyer E. *Noncontact Atomic Force Microscopy.* Springer, 2002.

[4] S. Fostner. Development of Metallic Electrodes on KBr. Master's thesis, McGill University, 2005.

[5] Helen G. Hansma and Jan H. Hoh. Biomolecularimaging with the atomic force microscope. *Annual Review of Biophysics and Biophysical Chemistry*, 23:15–39, 1994.

[6] Sarid D. *Scanning Force Microscopy.* Oxford University Press, 1991.

[7] Sader E.J. Experimental validation of theoretical models for the frequency response of atomic force microscope cantilever beams immersed in fluids. *Journal of Applied Physics.*, 87:3978, 2000.

[8] S.S. Rao. *Mechanical Vibrations, 3rd Edition.* Addison-Wesley, 1995.

[9] Green C.P. Sader E.J. Torsional frequency response of cantilever beams immersed in viscous fluids with applications to the atomic force microscope. *Journal of Applied Physics*, 92:6262, 2002.

[10] Nickolay V. Lavrik and Panos G. Datskos. Femtogram mass detection using photothermally actuated nanomechanical resonators. *Applied Physics Letters*, 82:16, 2003.

[11] Simon Scheuring Shirley A. Muller Daniel J. Muller, Dimitrios Fotiadis and Andreas Engel. Electrostatically balanced subnanometer imaging of biological specimens by atomic force microscope. *Biophysical Journal*, 76:1101–1111, 1999.

[12] Chu W.H. Technical report no. 2, dtmb. *Contract NObs-86396(X),*, Southwest Research Institute, 1963.

[13] Sader E.J. Frequency response of cantilever beams immersed in viscous fluids with applications to the atomic force microscope. *Journal of Applied Physics*, 84:64, 1998.

[14] T. Thundat D. P. Allison G. Y. Chen, R. J. Warmack and A. Huang. Resonance response of scanning force microscopy cantilevers. *Rev. Sci. Instrum.*, 65:2532, 1994.

[15] F. Ohnesorge D. A. Walters T. E. Schäffer, J. P. Cleveland and P. K. Hansma. Studies of vibrating atomic force microscope cantilevers in liquid. *Journal of Applied Physics.*, 80:3622, 1996.

[16] F.-J. Elmer and M. Dreier. Eigenfrequencies of a rectangular atomic force microscope cantilever in a medium. *Journal of Applied Physics.*, 81:7709, 1997.

[17] D. Xuefeng. Microfabrication using bulk wet etching with TMAH. Master's thesis, McGill University, 2005.

[18] Kei Kobayashi Kazumi Matsushinge Takeshi Fukuma, Masayuki Kimura and Hirofumi Yamada. Development of low noise cantilever deflection sensor for multienvironment frequency-modulation atomic force microscopy. *Review of Scientific Instruments*, 76:053704, 2005.

[19] Takeshi Fukuma and Suzanne P. Jarvis. Development of liquid-environment frequency modulation atomic force microscope with low noise deflection sensor for cantilevers of various dimensions. *Review of Scientific Instruments*, 77:043701, 2006.

[20] N.H.Thompson P.K.Hansma M.A.Wendman G.Gurley D. A.Walters, J.PCleveland and V.Elings. Short cantilevers for atomic force microscopy. *Review of Scientific Instruments*, 67:10, 1996.

[21] P.Mulvaney Sader E.J., I.Larson and L.R. White. Method for the calibration of atomic force microscope cantilevers. *Review of Scientific Instruments*, 66:7, 1995.

[22] R.Y. Steele R.J.Warmack P.I Oden, G.Y. Chen and T.Thundat. Viscous drag measurements utilizing microfabricated cantilevers. *Applied Physics Letters*, 68:26, 1996.

[23] United States Patent. Developer for positive photoresists. http://www.freepatentsonline.com/4576903.html.

[24] Ivaylo W. Rangelow. Reactive ion etching for microelectrical mechanical system fabrication. *J. Vac. Sci. Technol. B.*, 13:6, 1995.

[25] MEMS and Nanotechnology Exchange. Etching processes. http://cleanroom.byu.edu/rie_etching.phtml.

[26] MEMS and Nanotechnology Exchange. Etching processes. http://www.mems-exchange.org/MEMS/processes/etch.html.

[27] Martin G.R. Holdsworth B. *Digital Systems Reference Book*. Butterworth-Heinemann Ltd., 1993.

[28] H. Fuchs T. E. Schäffer. Optimized detection of normal vibration modes of atomic force microscope cantilevers with the optical beam deflection method. *Journal of Applied Physcs*, 97:083524, 2005.

[29] J. Philip A. Khan and P. Hess. Youngs modulus of silicon nitride used in scanning force microscope cantilevers. *Journal of Applied Physcs*, 95:4, 2004.

[30] Chung S. Hong S. Ryu K. Fan Z. Mirkin C. Liu C. Zhang M., Bulen D. A mems nanoplotter with high-density parallel dip-pen nanolithography probe arrays. *Nanotechnology*, 13:212–217, 2002.

[31] J. N. Newman. Propagation of water waves past long two-dimensional obstaclesd. *Journal of Fluid Mechanics*, 23:29, 1965.